

Higher-Order Total Directional Variation. Part I: Imaging Applications *

Simone Parisotto[†], Jan Lellmann[‡], Simon Masnou[§], and Carola-Bibiane Schönlieb[¶]

Abstract. We introduce a new class of higher-order anisotropic total variation regularizers which are defined for possibly inhomogeneous, smooth elliptic anisotropies. We propose a primal-dual hybrid gradient approach to approximate numerically the associated gradient flow. This choice of regularizers allows to preserve and enhance intrinsic anisotropic features in images. This is illustrated on various examples from different imaging applications: image denoising, wavelet-based image zooming, and reconstruction of surfaces from scattered height measurements.

Key words. Total directional variation, Anisotropy, Denoising, Wavelet-based zooming, Digital Elevation Map

AMS subject classifications. 47A52, 49M30, 49N45, 65J22, 94A08

1. Introduction. In the last decades, total variation (TV) regularisation has been successfully applied to a variety of imaging problems. In particular since [33], TV plays a crucial role for variational image denoising, image deblurring, inpainting, segmentation, magnetic resonance image (MRI) reconstruction and many others, see [12]. While the TV regulariser successfully eliminates noise and at the same time preserves characteristic image features like edges, it still has some shortcomings. A major one is the staircasing effect, resulting into blocky-like images [13, 36]. One approach to mitigate this effect is based on higher order total variation regularisers, e.g. [17, 18, 38, 44, 52], aiming to eliminate the staircasing effect by higher regularity in homogeneous regions of the image while still allowing for discontinuities in the presence of edges. The total generalized variation (TGV_{α}^Q) regulariser has been proposed in [11] to balance the first Q derivatives of u with a regularisation parameter vector α . Another modification of the TV regulariser has been the introduction of directional information in the regularisation, allowing to smooth images in an anisotropic fashion favouring preferred directions, e.g. [5, 54, 7, 21, 46, 25, 32, 30, 23, 22]. A recent combination of directional TV and higher-order derivatives is the directional total generalized variation [20] that equips the TGV_{α}^Q regulariser with one constant preferred smoothing direction.

In this paper we extend the directional total generalized variation [20] towards accommodating spatially-varying directional information by means of weighting the derivatives in the TGV_{α}^Q regulariser with 2-tensors. We show the effect of this new class of regularisers in different imaging applications where the introduced anisotropy plays a crucial role: im-

*Submitted to the editors DATE.

Funding: SP acknowledges UK EPSRC grant EP/L016516/1 for the University of Cambridge, Cambridge Centre for Analysis DTC. CBS acknowledges support from the EPSRC grants Nr. EP/M00483X/1, EP/K009745/1, the EPSRC centre EP/N014588/1, the Leverhulme Trust project 'Breaking the non-convexity barrier', the Alan Turing Institute TU/B/000071, the CHiPS (Horizon 2020 RISE project grant), the Isaac Newton Institute and the Cantab Capital Institute for the Mathematics of Information.

[†]CCA, University of Cambridge, Wilberforce Road, Cambridge CB3 0WA, UK (sp751@cam.ac.uk)

[‡]MIC, University of Lübeck, Maria-Goeppert-Straße 3, 23562 Lübeck, DE (jan.lellmann@mic.uni-luebeck.de)

[§]Université Claude Bernard Lyon 1, Institut Camille Jordan, Lyon, France (masnou@math.univ-lyon1.fr)

[¶]DAMTP, University of Cambridge, Wilberforce Road, Cambridge CB3 0WA, UK (cbs31@cam.ac.uk)

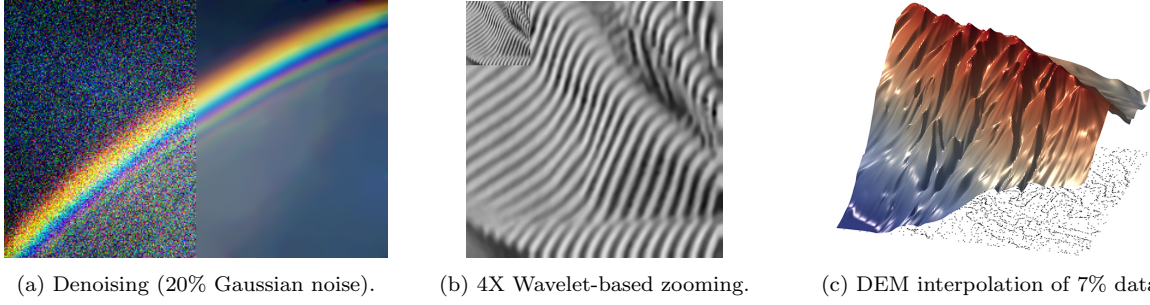


Figure 1: Imaging applications for the class of directional regularisers introduced in this paper.

age denoising, wavelet-based zooming and digital elevation map (DEM) interpolation with applications to atomic force microscopy (AFM) data, see [Figure 1](#).

To be more precise, what we propose is the following regulariser. Let $\Omega \subset \mathbb{R}^d$ be a bounded Lipschitz domain for $d \geq 1$ and $u : \Omega \rightarrow \mathbb{R}$ be function, then we investigate the higher-order directional total variation regularisation

$$(1) \quad \text{TDV}_{\alpha}^{\mathcal{Q}}(u, \mathcal{M}) := \sup_{\Psi} \left\{ \int_{\Omega} u \operatorname{div}_{\mathcal{M}}^{\mathcal{Q}} \Psi \, d\mathbf{x} \mid \text{for all } \Psi \in \mathcal{Y}_{\mathcal{M}, \alpha}^{\mathcal{Q}} \right\},$$

where \mathcal{Q} is the order of regularisation, \mathcal{M} is a collection of weighting fields, α is a vector of regularisation parameters, $\mathcal{T}^{\mathcal{Q}}(\mathbb{R}^d)$ is the vector space of \mathcal{Q} -tensors in \mathbb{R}^d and

$$(2) \quad \mathcal{Y}_{\mathcal{M}, \alpha}^{\mathcal{Q}} = \left\{ \Psi : \Psi \in C_c^{\mathcal{Q}}(\Omega, \mathcal{T}^{\mathcal{Q}}(\mathbb{R}^d)), \left\| \operatorname{div}_{\mathcal{M}}^j \Psi \right\|_{\infty} \leq \alpha_j, \forall j = 0, \dots, \mathcal{Q} - 1 \right\}.$$

We will provide the rigorous definition for (1) in [Section 2.2](#). We comment for now that the regulariser in (1) is designed for introducing weighted derivatives in the definition of $\text{TGV}_{\alpha}^{\mathcal{Q}}$. The anisotropy is introduced by a family of weights \mathcal{M} and a suitably weighted divergence $\operatorname{div}_{\mathcal{M}}^{\mathcal{Q}}$ of order \mathcal{Q} . Throughout the paper, we will consider a specific choice of \mathcal{M} that we call \mathcal{M}^a and that is given by

$$(3) \quad \mathcal{M}^a := (\mathbf{M}_j^a)_{j=1}^{\mathcal{Q}}, \text{ where } \mathbf{M}_j^a = \begin{cases} \mathbf{M}_j & \text{for } j > \mathcal{Q} - a; \\ \mathbf{I} & \text{for } j \leq \mathcal{Q} - a, \end{cases}$$

so as to weight all derivatives of order $q > \mathcal{Q} - a$ and keep the remaining derivatives unweighted.

1.1. Related work. In what follows we review the state-of-the-art that is most relevant for the newly proposed higher-order directional total variation regulariser. We focus in particular on functional regularizers but it is worth mentioning that there is a rich literature on fairly general anisotropic PDE models, mainly of first and second order, see for instance [\[41, 47, 50, 29, 9, 14, 3, 53\]](#) and the references therein. Our model can handle a more limited class of anisotropies but it can do it at any order of derivation, which is particularly useful in various applications.

The idea of anisotropic smoothing for imaging has certainly been pioneered by the book of Weickert on anisotropic diffusion equations [50]. Here, the structure tensor [27, 24, 28] is used to encode directional information. The structure tensor for a continuous imaging function $u : \Omega \rightarrow \mathbb{R}$ and non-negative parameters σ, ρ is defined as

$$(4) \quad \mathbf{J}_\rho(u) := K_\rho * (\nabla u_\sigma \otimes \nabla u_\sigma),$$

with $u_\sigma = K_\sigma * u$ and K_σ and K_ρ being Gaussian kernels with standard deviations σ and ρ , respectively. For $\nabla u_\sigma \neq 0$ the structure tensor $\mathbf{J}_\rho(u)$ has two orthogonal eigenvectors \mathbf{v}_1 and \mathbf{v}_2 with corresponding non-zero real eigenvalues $\lambda_1(\mathbf{x})$ and $\lambda_2(\mathbf{x})$. Here \mathbf{v}_1 and \mathbf{v}_2 approximately point in the direction ∇u_σ and $\nabla^\perp u_\sigma$. From this, diffusion tensors can be constructed which inherit \mathbf{v}_1 and \mathbf{v}_2 as eigenvectors but whose eigenvalues are expressions of λ_1 and λ_2 so to increase or reduce smoothing in these directions, compare for instance coherence-enhancing diffusion [51]. The concept of the structure tensor is used for variational regularisation by [46] in their proposed *single orientation estimation* approach. There, the authors consider a regulariser of the type

$$\int_{\Omega} w(\mathbf{x}) \mathbf{J}_\rho(u) \, d\mathbf{x},$$

for a non-negative weight function $w : \Omega \rightarrow \mathbb{R}$ and a continuous imaging function $u : \Omega \rightarrow \mathbb{R}$, for smoothing an image into a dominant single direction. For directed smoothing in two directions, the authors propose to estimate directions \mathbf{v}_1 and \mathbf{v}_2 as in [1] and, in their *double orientation estimation* approach, decompose $u(\mathbf{x}) = u_1(\mathbf{x}) + u_2(\mathbf{x})$ via

$$(5) \quad \min_u \alpha (\|\mathbf{v}_1^T \nabla u\|_1 + \|\mathbf{v}_2^T \nabla u\|_1) + \frac{1}{2} \|u - u^\diamond\|_2^2.$$

Let us also mention the work in [7] where oriented, local image structure is extracted from images by regularisers

$$(6) \quad \text{TV}^\alpha(u) = \int_{\Omega} |\mathbf{M}_\alpha \nabla u| \, d\mathbf{x},$$

with \mathbf{M}_α being the orthogonal rotation matrix for an angle $\alpha > 0$.

Another approach based on the analysis of eigenvalues and eigenvectors of the structure tensors can be found in [25]. The variational problem analysed there is

$$(7) \quad \min_u \alpha \int_{\Omega} ((\nabla u(\mathbf{x}))^T \mathbf{A}(u)(\mathbf{x}) \nabla u(\mathbf{x}))^{\frac{1}{2}} \, d\mathbf{x} + \frac{1}{2} \|u - u^\diamond\|_2^2.$$

Here, the anisotropy matrix $\mathbf{A} \in \text{Sym}^2(\Omega)$ is defined as

$$\mathbf{A}(u) := \mathbf{U}^T(\mathbf{x}) \text{diag}(\gamma(\lambda_1(\mathbf{x}) - \lambda_2(\mathbf{x})), 1) \mathbf{U}(\mathbf{x}), \quad \text{with} \quad \gamma(s) := (1 + s^2 \gamma_0^{-2})^{-1},$$

$\mathbf{J}_\rho(\mathbf{x}) = \mathbf{U}^T(\mathbf{x}) \mathbf{\Sigma}(\mathbf{x}) \mathbf{U}(\mathbf{x})$ the orthogonal decomposition of the structure tensor where $\mathbf{U}(\mathbf{x}) \in \mathbb{R}^{2 \times 2}$ is an orthogonal matrix and $\mathbf{\Sigma}(\mathbf{x}) := \text{diag}(\lambda_1(\mathbf{x}), \lambda_2(\mathbf{x})) \in \mathbb{R}^{2 \times 2}$ is the diagonal matrix of the ordered eigenvalues λ_1 and λ_2 . Further, in [5], a discrete *directional total variation*

($\text{TV}_{a,\theta}$) regulariser for denoising discrete images \mathbf{u} with a single dominant direction (directional images) is introduced via affine transformations of test functions: the circular unit ball generated by the L^2 -norm is transformed into an ellipse $E^{a,\theta}$, with mayor semiaxis $a > 1$ rotated by θ , penalizing variations for large a along θ :

$$(8) \quad \text{TV}_{a,\theta}(\mathbf{u}) = \sum_{i,j} \sup_{\Psi \in E^{a,\theta}} \langle (\nabla \mathbf{u})_{i,j}, \Psi \rangle.$$

A straightforward generalization of (8) is to spatially vary the direction θ in multiple directions, namely $\boldsymbol{\theta} := \theta(\mathbf{x})$. In [54] the authors propose to adapt $\boldsymbol{\theta}$ to the edge directions,

$$(9) \quad (\cos \boldsymbol{\theta}, \sin \boldsymbol{\theta}) = \frac{(\nabla u_\sigma)^\perp}{\|\nabla u_\sigma\|_2},$$

so as to associate at each pixel position (i, j) a specific ellipsoid ball $E^{a,\theta_{ij}}$ for the test functions, leading to the discrete *edge adaptive directional total variation* (EADTV) regulariser:

$$(10) \quad \text{EADTV}_{\alpha,\boldsymbol{\theta}}(\mathbf{u}) = \sum_{i,j} \sup_{\Psi \in E^{\alpha,\theta_{ij}}} \langle (\nabla \mathbf{u})_{i,j}, \Psi \rangle.$$

In [32], an admissible set of test functions are locally adapted to the geometry of \mathbf{u} via the regulariser

$$(11) \quad \sigma_{\mathcal{C}} = \sup_{\mathbf{v} \in \mathcal{C}} \langle \mathbf{u}, \mathbf{v} \rangle,$$

with $\mathcal{C} = \mathbf{L}\mathcal{D} = \{\mathbf{v} : \mathbf{v} = \mathbf{L}\mathbf{p}, \mathbf{p} \in \mathcal{D}\}$ and $\mathcal{D} = \{\mathbf{p} \in \mathbb{R}^{d\ell} : \mathbf{p} \in \mathcal{D}_{\text{loc}}^i \in \mathbb{R}^d, i = 1, \dots, \ell\}$, where $\mathbf{L} \in \mathbb{R}^{\ell \times d\ell}$ is a discretisation of the divergence operator div , $\mathbf{p} \in \mathbb{R}^{d\ell}$, and $\mathcal{D}_{\text{loc}}^i$ is the local constraint set for each $\mathbf{p}_i \in \mathbb{R}^d$, $i = 1, \dots, \ell$. When $\mathcal{D}_{\text{loc}}^i := B_\alpha(\mathbf{0}) \subset \mathbb{R}^d$, with $B_\alpha(\mathbf{0})$ the ball of radius α centred at $\mathbf{0}$, then $\sigma_{\mathcal{C}}(\mathbf{u}) \equiv \alpha \text{TV}(\mathbf{u})$. In [30], the *structure tensor total variation* (STV) focuses on the nuclear norm of the structure tensor $\mathbf{J}_\rho(\mathbf{u})$ from (4) in order to measure the local image variation:

$$(12) \quad \text{STV}_p(u) = \left\| \left(\sqrt{\lambda_1}, \sqrt{\lambda_2} \right) \right\|_p,$$

where $\lambda_1 \geq \lambda_2$ are the ordered eigenvalues of $\mathbf{J}_\rho(u)$. Also in [23], a regulariser is proposed whose smoothing directions vary according to the image content, leading to the analysis of

$$\mathcal{R}_{\mathbf{J}}(u) = g_\gamma(\mathbf{S} \nabla u), \quad \mathbf{S} = \max \left(\sqrt{\gamma}, \sqrt[4]{\lambda_1 + \lambda_2} \Lambda^{-0.5} \mathbf{Q}^T \right),$$

where g_γ is the Huber regularisation with parameter $\gamma > 0$ and the structure tensor \mathbf{J}_ρ is decomposed as $\mathbf{J}_\rho = \mathbf{Q}\mathbf{\Lambda}\mathbf{Q}^T$. In [22], a discrete weighted *directional Total Variation* (dTV) regulariser is introduced as

$$(13) \quad \text{dTV}(\mathbf{u}) = \sum_{n=1}^N |\mathcal{P}_{\boldsymbol{\xi}_n} \nabla u_n|, \quad \text{with} \quad \boldsymbol{\xi}_n := \nabla u_n / (K_\sigma * |\nabla u_n|),$$

by projecting onto the complementary part of a vector field $\mathcal{P}_{\xi_n} \mathbf{x} = \mathbf{x} - \langle \xi_n, \mathbf{x} \rangle \xi_n$.

In [20], the continuous *directional total variation* (DTV) and *directional total generalized variation* (DTGV) are analysed for a single global direction θ :

$$(14) \quad \text{DTV}(u) = \sup_{\tilde{\Psi}} \left\{ \int_{\Omega} u \operatorname{div} \tilde{\Psi} \, d\mathbf{x} \mid \Psi \in C_c^1(\Omega, \mathbb{R}^2), \tilde{\Psi}(\mathbf{x}) \in E^{a,\theta}(\mathbf{0}), \forall \mathbf{x} \in \Omega \right\},$$

$$(15) \quad \text{DTGV}_{\alpha}^Q(u) = \sup_{\tilde{\Psi}} \left\{ \int_{\Omega} u \operatorname{div}^Q \tilde{\Psi} \, d\mathbf{x} \mid \begin{array}{l} \Psi \in C_c^Q(\Omega, \operatorname{Sym}^Q(\mathbb{R}^2)), \\ \|\operatorname{div}^q \tilde{\Psi}(\mathbf{x})\| \leq \alpha_\ell, \forall q = 0, \dots, Q-1 \end{array} \right\},$$

where \mathbf{R}_θ and $\mathbf{\Lambda}_a$ are rotation and contraction matrices, respectively, and test functions are

$$E^{a,\theta}(\mathbf{0}) \ni \tilde{\Psi}(\mathbf{x}) = \mathbf{R}_\theta \mathbf{\Lambda}_a \Psi(\mathbf{x}), \quad \text{with } \Psi \in B_1(\mathbf{0}).$$

1.2. Our proposal. Our work extends the regularisers in (14)-(15) for handling multiple directions θ in $\Omega \subset \mathbb{R}^2$. We investigate the directional total variation regulariser of (1) and study its performance for a variety of image processing problems by solving

$$(16) \quad u^* \in \arg \min_u \sum_{q=1}^Q \text{TDV}_{\alpha_q}^q(u, \mathcal{M}_q) + \frac{\eta}{2} \|\mathcal{S}u - u^\diamond\|_2^2,$$

where $u^\diamond \in L^2(\Omega)$ is a given, imperfect and possibly incomplete imaging data, and $\mathcal{S} : L^2(\Omega) \rightarrow L^2(\Omega)$ a linear operator. We consider the cases for which \mathbf{M}_j in $\mathcal{M}_q = (\mathbf{M}_j)_{j=1}^q$ from (1) is

$$\text{either } \mathbf{M}_j = \mathbf{I} \quad \text{or} \quad \mathbf{M}_j = \mathbf{\Lambda}_b(\mathbf{R}_\theta)^T,$$

for \mathbf{I} the identity matrix and $\mathbf{\Lambda}_b$, \mathbf{R}_θ contraction and rotation matrices, respectively, with

$$\mathbf{\Lambda}_b = \begin{pmatrix} b_1(\mathbf{x}) & 0 \\ 0 & b_2(\mathbf{x}) \end{pmatrix} \quad \text{and} \quad \mathbf{R}_\theta = \begin{pmatrix} \cos \theta(\mathbf{x}) & -\sin \theta(\mathbf{x}) \\ \sin \theta(\mathbf{x}) & \cos \theta(\mathbf{x}) \end{pmatrix},$$

with $\mathbf{b} := (b_1(\mathbf{x}), b_2(\mathbf{x}))^T \in [0, 1]^2$ and $\theta := \theta(\mathbf{x}) \in [0, 2\pi)$: Occasionally, we will identify with $\mathbf{v} : \Omega \rightarrow \mathbb{R}^2$ the vector field associated to the angle θ , i.e. $\mathbf{v} = (\cos \theta, \sin \theta)^T$ and with $\mathbf{v}_\perp = (-\sin \theta, \cos \theta)^T$ its orthogonal. Thus, we interpret the core operation of the dual version of the regulariser in (1), $\mathbf{M}_1 \nabla \otimes u$, as directional derivatives of u along \mathbf{v} and \mathbf{v}_\perp since

$$(17) \quad \mathbf{M}_1 \nabla \otimes u = \mathbf{\Lambda}_b(\mathbf{R}_\theta)^T \nabla \otimes u = \begin{pmatrix} b_1 \nabla_{\mathbf{v}} u \\ b_2 \nabla_{\mathbf{v}_\perp} u \end{pmatrix}.$$

We will in particular focus on the case $\mathbf{b} = (1, b_2(\mathbf{x}))$ for $b_2(\mathbf{x}) \in [0, 1]$ both fixed $b_2(\mathbf{x}) = \varepsilon \rightarrow 0$ and varying in Ω , see Remark 1.1 for the geometrical interpretation.

Remark 1.1. In Figure 2 we simulate the two dimensional behaviour of (17) for different choices of b_2 . More precisely, for a continuous imaging function $u : \Omega \rightarrow \mathbb{R}$ we represent a possible situation at the position $\mathbf{x} \in \Omega$ of the vectors $\mathbf{p} = \nabla u$, $\mathbf{p} = (p_1, p_2)$, and $\mathbf{v} = (v_1, v_2)$, depicted with red and blue arrows, respectively. We also represent the components

$\mathbf{r} = (r_1, r_2) = (p_1 v_1, p_2 v_2)$ of $\nabla_{\mathbf{v}} u = r_1 + r_2 = p_1 v_1 + p_2 v_2$ by a green arrow. We kept these values fixed from Figure 2a to Figure 2f. Moreover, the test functions $\Psi = (\Psi^1, \Psi^2)$ lie on the black circle due to the constraint $\|\Psi\|_2 \leq 1$. Note that in the 2D domain we have

$$\mathbf{M}_1 \nabla u \cdot \Psi = \nabla u \cdot \mathbf{M}_1^T \Psi,$$

which allows to change the metric space of the test functions into an elliptic ball in magenta. Thus, for a fixed $b_1 = 1$, b_2 is set to vary between 0 and 1. Finally, the magenta arrow corresponds to the direction of Ψ which realizes the supremum of the regulariser TDV_{α}^1 in Equation (1). We observe in Figure 2f the limit case $\mathbf{b} = (1, 0)$ where $\text{TDV}_{\alpha}^1(u, \mathcal{M})$ penalizes the rate of change of u only along \mathbf{v} without orthogonal \mathbf{v}_{\perp} contribution. In all the other circumstances, \mathbf{v}_{\perp} act as quality estimation of \mathbf{v} , leading to a full isotropic approach in the case $\mathbf{b} = (1, 1)$ of Figure 2a, since the magenta arrow is bended in the direction of the gradient ∇u rather than the direction of $\nabla_{\mathbf{v}} u$.

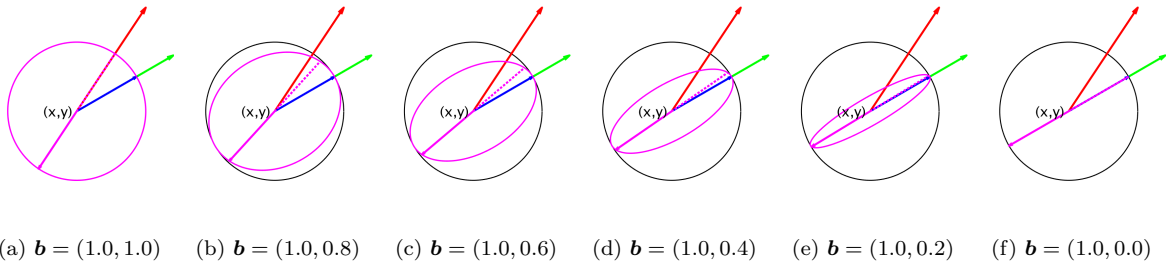


Figure 2: Different choices for $\mathbf{b} = (1, b_2)$ in $\text{TDV}_{\alpha}^1(u, \mathcal{M})$, with $\mathcal{M} = \mathbf{\Lambda}_{\mathbf{b}}(\mathbf{R}_{\theta})^T$ and θ fixed.

1.3. Contribution of the paper. In what follows we will derive a rigorous definition of the total directional regulariser (1); a characterisation of (1) that turns (16) amenable for numerical solution: for the latter we propose a primal-dual algorithm and present certain instances for different combinations of orders $q = 1, \dots, Q$, up to $Q = 3$ in (1); a number of numerical experiments with this new regulariser for image denoising, image zooming and interpolation of two-dimensional surfaces from a sparse number of given height values.

1.4. Organization of the paper. In Section 2 we discuss the higher-order total directional variation regularisers with anisotropy. The numerical details of the discretisation are introduced in Section 3, with the primal-dual algorithm and the numerical optimisation described in Section 4. Imaging applications to denoising, wavelet-based zooming and surface interpolation with application to atomic force microscopy imaging are discussed in Section 5.

2. Higher-order total directional variation. In this section we introduce the rigorous definition of (1). To do so, we first introduce the terminology of tensors and their mathematical manipulation.

2.1. Tensors. Following [11], let $\mathcal{T}^\ell(\mathbb{R}^d)$ be the vector space of ℓ -tensors defined as

$$\mathcal{T}^\ell(\mathbb{R}^d) := \left\{ \boldsymbol{\xi} : \underbrace{\mathbb{R}^d \times \cdots \times \mathbb{R}^d}_{\ell\text{-times}} \rightarrow \mathbb{R}, \text{ such that } \boldsymbol{\xi} \text{ is } \ell\text{-linear} \right\}.$$

On $\mathcal{T}^\ell(\mathbb{R}^d)$, we have the following operations:

- let \otimes be the tensor product for $\boldsymbol{\xi}_1 \in \mathcal{T}^{\ell_1}(\mathbb{R}^d)$, $\boldsymbol{\xi}_2 \in \mathcal{T}^{\ell_2}(\mathbb{R}^d)$, with $\boldsymbol{\xi}_1 \otimes \boldsymbol{\xi}_2 \in \mathcal{T}^{\ell_1+\ell_2}(\mathbb{R}^d)$:

$$(\boldsymbol{\xi}_1 \otimes \boldsymbol{\xi}_2)(\mathbf{a}_1, \dots, \mathbf{a}_{\ell_1+\ell_2}) = \boldsymbol{\xi}_1(\mathbf{a}_1, \dots, \mathbf{a}_{\ell_1}) \boldsymbol{\xi}_2(\mathbf{a}_{\ell_1+1}, \dots, \mathbf{a}_{\ell_1+\ell_2});$$

- let $\text{trace}(\boldsymbol{\xi}) \in \mathcal{T}^{\ell-2}(\mathbb{R}^d)$ be the trace of $\boldsymbol{\xi} \in \mathcal{T}^\ell(\mathbb{R}^d)$, with $\ell \geq 2$, defined by

$$\text{trace}(\boldsymbol{\xi})(\mathbf{a}_1, \dots, \mathbf{a}_{\ell-2}) = \sum_{i=1}^d \boldsymbol{\xi}(\mathbf{e}_i, \mathbf{a}_1, \dots, \mathbf{a}_{\ell-2}, \mathbf{e}_i),$$

where \mathbf{e}_i is the i -th standard basis vector;

- let $(\cdot)^\sim$ be such that if $\boldsymbol{\xi} \in \mathcal{T}^\ell(\mathbb{R}^d)$, then $\boldsymbol{\xi}^\sim(\mathbf{a}_1, \dots, \mathbf{a}_\ell) = \boldsymbol{\xi}(\mathbf{a}_\ell, \mathbf{a}_1, \dots, \mathbf{a}_{\ell-1})$;
- let $(\cdot)^\bar{}$ be such that if $\boldsymbol{\xi} \in \mathcal{T}^\ell(\mathbb{R}^d)$, then $\boldsymbol{\xi}^\bar{}(\mathbf{a}_1, \dots, \mathbf{a}_\ell) = \boldsymbol{\xi}(\mathbf{a}_\ell, \dots, \mathbf{a}_1)$;
- let $\boldsymbol{\xi}, \boldsymbol{\eta} \in \mathcal{T}^\ell(\mathbb{R}^d)$. Thus $\mathcal{T}^\ell(\mathbb{R}^d)$ is equipped with the scalar product defined as

$$\boldsymbol{\xi} \cdot \boldsymbol{\eta} = \sum_{p \in \{1, \dots, d\}^\ell} \xi_{p_1, \dots, p_\ell} \eta_{p_1, \dots, p_\ell}.$$

We now introduce the derivative operator for tensors and its weighted version.

Definition 2.1. Let $\nabla = (\partial_1, \dots, \partial_d)^\top$ be the derivative operator and $\boldsymbol{\xi} \in \mathcal{T}^\ell(\mathbb{R}^d)$. The derivative of $\boldsymbol{\xi}$ is defined as $(\nabla \otimes \boldsymbol{\xi}) \in \mathcal{T}^{\ell+1}(\mathbb{R}^d)$ via the following:

$$\nabla \otimes \boldsymbol{\xi} := (\nabla \otimes \boldsymbol{\xi})_{j, i_1, \dots, i_\ell} = \partial_j \xi_{i_1, \dots, i_\ell}.$$

Let $\boldsymbol{\eta} \in \mathcal{T}^2(\mathbb{R}^d)$. The derivative operator weighted by $\boldsymbol{\eta}$ is defined as $\boldsymbol{\eta} \nabla \in \mathcal{T}^1(\mathbb{R}^d)$ and the derivative of $\boldsymbol{\xi} \in \mathcal{T}^\ell(\mathbb{R}^d)$ weighted by $\boldsymbol{\eta}$ is defined as $(\boldsymbol{\eta} \nabla \otimes \boldsymbol{\xi}) \in \mathcal{T}^{\ell+1}(\mathbb{R}^d)$ via the following:

$$\boldsymbol{\eta} \nabla \otimes \boldsymbol{\xi} := (\boldsymbol{\eta} \nabla \otimes \boldsymbol{\xi})_{j, i_1, \dots, i_\ell} = \sum_{k=1}^d \eta_{j,k} \partial_k \xi_{i_1, \dots, i_\ell}.$$

In the next, we will also denote the space of $\mathcal{T}^\ell(\mathbb{R}^d)$ -valued tensors Q -times uniformly continuously differentiable as $C^Q(\Omega, \mathcal{T}^\ell(\mathbb{R}^d))$ which is a Banach space with the norm

$$\|u\|_{\infty, Q} = \max_{\ell=0, \dots, Q} \sup_{\mathbf{x} \in \Omega} \left| \nabla^\ell \otimes u(\mathbf{x}) \right|,$$

where $(\nabla^Q \otimes u) : \Omega \rightarrow \mathcal{T}^{Q+\ell}(\mathbb{R}^d)$ and the space $C_c^Q(\Omega, \mathcal{T}^\ell(\mathbb{R}^d))$ of $\mathcal{T}^\ell(\mathbb{R}^d)$ -valued tensors Q -times continuously differentiable with compact support in Ω .

2.2. Definition of total directional variation. For making sense of the distributional formulation of higher-order directional variation in (1) we need an integration by parts formula for the weighted derivative of tensors in Definition 2.1. Namely we consider

$$\int_{\Omega} (\mathbf{M} \nabla \otimes \mathbf{A}) \cdot \Psi \, dx,$$

with $\Omega \subset \mathbb{R}^d$ be a bounded Lipschitz domain, $\mathbf{M} \in C^1(\Omega, \mathcal{T}^2(\mathbb{R}^d))$, $\mathbf{A} \in C^1(\Omega, \mathcal{T}^\ell(\mathbb{R}^d))$ and $\Psi \in C_c^1(\Omega, \mathcal{T}^{\ell+1}(\mathbb{R}^d))$. We report in this sections the main results from the second part of this work [39], without the detailed proofs. Firstly, we explore the action of \mathbf{M} on Ψ :

Lemma 2.2. *Let Ω , \mathbf{M} , \mathbf{A} and Ψ as above. Then:*

$$(18) \quad \int_{\Omega} (\mathbf{M} \nabla \otimes \mathbf{A}) \cdot \Psi \, dx = \int_{\Omega} (\nabla \otimes \mathbf{A}) \cdot \text{trace}(\mathbf{M} \otimes \Psi^\sim), \text{ for all } \mathbf{M}, \mathbf{A}, \Psi \, dx.$$

Thus, the adjoint property follows:

Lemma 2.3. *Let Ω , \mathbf{M} , \mathbf{A} and Ψ as above. Then:*

$$(19) \quad \int_{\Omega} (\mathbf{M} \nabla \otimes \mathbf{A}) \cdot \Psi \, dx = - \int_{\Omega} \mathbf{A} \cdot \text{div}_{\mathbf{M}} \Psi \, dx, \text{ for all } \mathbf{M}, \mathbf{A}, \Psi,$$

where $\text{div}_{\mathbf{M}} \Psi := \text{trace}(\nabla \otimes [\text{trace}(\mathbf{M} \otimes \Psi^\sim)]^\sim)$.

We can now define the *total directional variation* of order Q with weights $\alpha \in \mathbb{R}_+^Q$.

Definition 2.4. *Let $\Omega \subset \mathbb{R}^d$, $u \in L^1(\Omega, \mathbb{R})$, $Q \in \mathbb{N}$, $\mathcal{M} := (\mathbf{M}_j)_{j=1}^Q$ be a collection of fields in $C^\infty(\Omega, \mathcal{T}^2(\mathbb{R}^d))$ and $\alpha := (\alpha_0, \dots, \alpha_{Q-1})$ be a positive weight vector. Then, the total directional variation of order Q , associated with \mathcal{M} and α , is defined as:*

$$(20) \quad \text{TDV}_{\alpha}^Q(u, \mathcal{M}) := \sup_{\Psi} \left\{ \int_{\Omega} u \, \text{div}_{\mathcal{M}}^Q \Psi \, dx \mid \text{for all } \Psi \in \mathcal{Y}_{\mathcal{M}, \alpha}^Q \right\},$$

where

$$(21) \quad \mathcal{Y}_{\mathcal{M}, \alpha}^Q = \left\{ \Psi : \Psi \in C_c^Q(\Omega, \mathcal{T}^Q(\mathbb{R}^d)), \left\| \text{div}_{\mathcal{M}}^j \Psi \right\|_{\infty} \leq \alpha_j, \forall j = 0, \dots, Q-1 \right\}$$

and the weighted divergence of order q is defined recursively, from Lemma 2.3, as:

$$(22) \quad \begin{aligned} \text{div}_{\mathcal{M}}^0 \Psi &:= \Psi, & \text{if } j = 0, \\ \text{div}_{\mathcal{M}}^1 \Psi &:= \text{div}_{\mathbf{M}_Q} \Psi, & \text{if } j = 1, \\ &\vdots & \vdots \\ \text{div}_{\mathcal{M}}^Q(\Psi) &:= \text{div}_{\mathbf{M}_{Q-j+1}} \left(\text{div}_{\mathcal{M}}^{j-1} \Psi \right) & \text{if } j = 2, \dots, Q. \end{aligned}$$

Remark 2.5. For $\mathcal{M} = (\mathbf{I})_{j=1}^Q$, then $\text{TDV}_{\alpha}^Q(u, \mathcal{M}) \equiv \neg\text{symTG}_{\alpha}^Q(u)$, [11, Remark 3.10].

2.3. Directional matrices for applications. In what follows, we introduce a particular parametrisation of directional matrices for fields \mathcal{M} in (20). For standard imaging applications, we will usually deal with grey-scale images $u : \Omega \rightarrow \mathbb{R}$, $\Omega \subset \mathbb{R}^2$, i.e. $d = 2$.

Definition 2.6 (Directional matrices). Let $(\mathbf{b}^j)_{j=1}^Q$, $\mathbf{b}^j : \Omega \rightarrow [0, 1]^2$, be a collection of so-called contraction functions, $(\boldsymbol{\theta}^j)_{j=1}^Q$, $\boldsymbol{\theta}^j : \Omega \rightarrow [0, 2\pi)$, be a collection of angles, and $\boldsymbol{\Lambda}_{\mathbf{b}}^j$ and $\mathbf{R}_{\boldsymbol{\theta}}^j$ the associated contraction and rotation matrices, respectively, defined as

$$\boldsymbol{\Lambda}_{\mathbf{b}}^j := \begin{pmatrix} \mathbf{b}_1^j & 0 \\ 0 & \mathbf{b}_2^j \end{pmatrix}, \quad \mathbf{R}_{\boldsymbol{\theta}}^j := \begin{pmatrix} \cos \boldsymbol{\theta}^j & -\sin \boldsymbol{\theta}^j \\ \sin \boldsymbol{\theta}^j & \cos \boldsymbol{\theta}^j \end{pmatrix} \in \text{SO}(2).$$

Then we define $\mathcal{M} := (\mathbf{M}_j)_{j=1}^Q$ to be a collection of contraction-rotation matrices

$$\mathbf{M}_j := \boldsymbol{\Lambda}_{\mathbf{b}}^j (\mathbf{R}_{\boldsymbol{\theta}}^j)^\top = \left(\lambda_{pk}^j r_{\ell k}^j \right)_{p,\ell},$$

where $\lambda_{pk}^j, r_{\ell k}^j$ are the element-wise entries of the matrices $\boldsymbol{\Lambda}_{\mathbf{b}}^j, \mathbf{R}_{\boldsymbol{\theta}}^j$, respectively.

Definition 2.7 (Weighted derivatives of order 1). Let $\nabla = (\partial_1, \partial_2)^\top$ be the derivative operator, such that the gradient of u is defined by $\nabla u := \nabla \otimes u = (\partial_1 u, \partial_2 u)^\top$. Then, the weighted derivative operator of order 1 associated to the directional matrix \mathbf{M}_1 from Definition 2.6 is

$$\mathbf{M}_1 \nabla u := (\mathbf{M}_1 \nabla \otimes u)_p = \lambda_{pk}^1 r_{\ell k}^1 \partial_\ell u.$$

Remark 2.8. If $\mathbf{M} = \mathbf{I}$ (i.e. $b_1^1 \equiv b_2^1 \equiv 1$ and $\boldsymbol{\theta}^q \equiv 0$ for all $\mathbf{x} \in \Omega$), then $\mathbf{M}_1 \nabla u \equiv \nabla u$.

Remark 2.9. Let $\mathbf{v}^1 = (\cos \boldsymbol{\theta}^1, \sin \boldsymbol{\theta}^1)$ be a vector field associated to the angle $\boldsymbol{\theta}^1$ and let $\mathbf{v}_\perp^1 = (-\sin \boldsymbol{\theta}^1, \cos \boldsymbol{\theta}^1)$ be its orthogonal field. Then

$$\mathbf{M}_1 \nabla \otimes u := \begin{pmatrix} \mathbf{b}_1^1 \nabla_{\mathbf{v}^1} u \\ \mathbf{b}_2^1 \nabla_{\mathbf{v}_\perp^1} u \end{pmatrix},$$

where $\nabla_{\mathbf{z}} u$ represents the directional derivative along a vector field \mathbf{z} , defined as

$$\nabla_{\mathbf{z}} u(\mathbf{x}) = \nabla u(\mathbf{x}) \cdot \mathbf{z} = \sum_{i=1}^2 \partial_i u z_i.$$

Definition 2.10 (Weighted derivatives of order Q). We define the derivative of order Q of u using Definition 2.7 recursively as

$$\nabla^Q u := (\nabla \otimes \nabla^{Q-1} u)_{p_Q, \dots, p_1} = \partial_{p_Q} \dots \partial_{p_1} u.$$

We define the weighted derivative of order Q of u with respect to \mathcal{M} recursively as

$$\nabla_{\mathcal{M}}^0 u := u,$$

$$\nabla_{\mathcal{M}}^1 u := (\mathbf{M}_1 \nabla \otimes u)_{p_1} = \lambda_{p_1 k}^1 r_{\ell k}^1 \partial_\ell u,$$

\vdots

$$\nabla_{\mathcal{M}}^Q u := ((\mathbf{M}_Q \nabla) \otimes (\mathbf{M}_{Q-1} \nabla^{Q-1} u))_{p_Q, \dots, p_1} = \lambda_{p_Q k_Q}^Q r_{\ell_Q k_Q}^Q \partial_{\ell_Q} (\mathbf{M}_{Q-1} \nabla^{Q-1} \otimes u)_{p_{Q-1}, \dots, p_1}.$$

With these definitions we can now make (3) more precise.

Definition 2.11. Let $a \in [0, Q]$ be such that $a \in \mathbb{N}$ and let \mathcal{M}^a be a collection of fields in $C^\infty(\Omega, \mathcal{T}^2(\mathbb{R}^d))$ defined starting from \mathcal{M} as follows

$$(23) \quad \mathcal{M}^a := (\mathbf{M}_j^a)_{j=1}^Q, \text{ where } \mathbf{M}_j^a = \begin{cases} \mathbf{M}_j & \text{for } j > Q - a; \\ \mathbf{I} & \text{for } j \leq Q - a. \end{cases}$$

Then, \mathcal{M}^a represents the derivatives weights: for $j = 1, \dots, Q - a$ we will consider classic derivatives. In the next, we will refer to a as anisotropy order.

We can now define the total directional variation of order Q and anisotropy a , with \mathcal{M}^a as in Definition 2.11 and weights $\alpha \in \mathbb{R}_+^Q$.

Definition 2.12. We call total directional variation of order Q and anisotropy a the regulariser $\text{TDV}_\alpha^Q(u, \mathcal{M}^a)$ in Definition 2.4 with weights \mathcal{M}^a as in Definition 2.11.

2.4. Examples. We present some examples of the total directional variation of order Q for $Q = 1, 2, 3$, anisotropy $a = 1$, and directional matrices $\mathbf{M}_j \equiv \mathbf{M} = \Lambda_b(\mathbf{R}_\theta)^\top$ as in Definition 2.6. That is, we focus on the following cases:

- order $Q = 1$ and anisotropy $a = 1$, $\mathcal{M}^1 = \mathbf{M}$:

$$\begin{aligned} \text{TDV}_\alpha^1(u, \mathcal{M}^1) &:= \sup_{\Psi} \left\{ \int_{\Omega} u \operatorname{div}_{\mathbf{M}} \Psi \, d\mathbf{x} \mid \text{for all } \Psi \in \mathcal{Y}_{\mathcal{M}^1, \alpha}^1 \right\}; \\ \mathcal{Y}_{\mathcal{M}^1, \alpha}^1 &= \{ \Psi : \Psi \in C_c^\infty(\Omega, \mathbb{R}^2), \|\Psi\|_\infty \leq \alpha_0 \}; \end{aligned}$$

- order $Q = 2$ and anisotropy $a = 1$, $\mathcal{M}^1 = (\mathbf{I}, \mathbf{M})$:

$$\begin{aligned} \text{TDV}_\alpha^2(u, \mathcal{M}^1) &:= \sup_{\Psi} \left\{ \int_{\Omega} u \operatorname{div}(\operatorname{div}_{\mathbf{M}} \Psi) \, d\mathbf{x} \mid \text{for all } \Psi \in \mathcal{Y}_{\mathcal{M}^1, \alpha}^2 \right\}; \\ \mathcal{Y}_{\mathcal{M}^1, \alpha}^2 &= \{ \Psi : \Psi \in C_c^Q(\Omega, \mathbb{R}^{2 \times 2}), \|\Psi\|_\infty \leq \alpha_0, \|\operatorname{div}_{\mathbf{M}} \Psi\|_\infty \leq \alpha_1 \}; \end{aligned}$$

- order $Q = 3$ and anisotropy $a = 1$, $\mathcal{M}^1 = (\mathbf{I}, \mathbf{I}, \mathbf{M})$:

$$\begin{aligned} \text{TDV}_\alpha^3(u, \mathcal{M}^1) &:= \sup_{\Psi} \left\{ \int_{\Omega} u \operatorname{div}^2(\operatorname{div}_{\mathbf{M}} \Psi) \, d\mathbf{x} \mid \text{for all } \Psi \in \mathcal{Y}_{\mathcal{M}^1, \alpha}^3 \right\}; \\ \mathcal{Y}_{\mathcal{M}^1, \alpha}^3 &= \left\{ \Psi : \Psi \in C_c^Q(\Omega, \mathbb{R}^{2 \times 2 \times 2}), \|\Psi\| \leq \alpha_0, \|\operatorname{div}_{\mathbf{M}} \Psi\| \leq \alpha_1, \|\operatorname{div}(\operatorname{div}_{\mathbf{M}} \Psi)\|_\infty \leq \alpha_2 \right\}. \end{aligned}$$

3. Numerical discretisation. The rest of the paper focuses on the discretised formulation of (16), its numerical solution and performance on a number of image processing examples. We start by introducing the discretisation of (16).

3.1. Staggered grids. We will discretise (16) by means of finite-differences on two staggered regular Cartesian grids of width $h > 0$, one located on the grid vertices, named *grid of pixels* Ω^h , and one in the centre of the squares, called *grid of cell centres* Γ^h :

$$\begin{aligned} \Omega^h &= \{(ih, jh) \mid (1, 1) \leq (i, j) \leq (M, N)\}, \\ \Gamma^h &= \left\{ (\tilde{k}h, \tilde{l}h) \mid (\tilde{k}, \tilde{l}) = \left(k + \frac{1}{2}, l + \frac{1}{2} \right), (1, 1) \leq (k, l) < (M, N) \right\}, \end{aligned}$$

where Ω^h is of size $M \times N$, Γ^h is of size $(M-1) \times (N-1)$ and the pairs $(i, j) \in \mathbb{N}^2$, $(k, l) \in \mathbb{N}^2$ are the indices denoting the positions (ih, jh) , $(\tilde{k}h, \tilde{l}h)$ on the grids Ω^h and Γ^h , respectively. The grid Γ^h will be used to perform the weighted derivative operation, i.e. for introducing the anisotropy. Moreover, let $\boldsymbol{\iota} = (\iota_1, \dots, \iota_Q)$ be a multi-index variable with $\iota_j \in \{1, 2\}$, indicating the partial derivatives involved in the derivative of order Q . Let further $X_{\boldsymbol{\iota}}^{j,h}$ be the grids of width h where the discrete j -th order derivatives with respect to the multi-variable $\boldsymbol{\iota}$ are located. Note that for $Q = 0$ we have $X_{\boldsymbol{\iota}}^{0,h} \equiv \Omega^h$.

3.2. Discretised objects. By means of the superscript h , we define the finite-dimensional approximation of the following quantities, where $|\Omega_h|$, $|\Gamma_h|$ and $|X_{\boldsymbol{\iota}}^{j,h}|$ are the number of grid points in Ω_h , Γ_h and $X_{\boldsymbol{\iota}}^{j,h}$, respectively:

- $\mathbf{u}^h \in \mathbb{R}^{|\Omega^h|}$ is the discretisation of the function u ;
- $\mathbf{u}^{\diamond,h}$ is the discretisation of the observed imaging data u^{\diamond} ;
- $\mathbf{v}^h = (\mathbf{v}_1^h, \mathbf{v}_2^h) \in \mathbb{R}^{|\Gamma^h \times \Gamma^h|}$ is a discrete vector field;
- $\mathbf{b}^h = (\mathbf{b}_1^h, \mathbf{b}_2^h) \in \mathbb{R}^{|\Gamma^h \times \Gamma^h|}$ are discrete contraction weights for $\Lambda_{\mathbf{b}}$;
- $\mathcal{M}_q^h = (\mathbf{M}_{q,j}^h)_{j=1}^Q$ discretises the collection of weights $\mathcal{M}_q = (\mathbf{M}_{q,j})_{j=1}^Q$, where each $\mathbf{M}_{q,j}^h \in \mathbb{R}^{|\Gamma^h \times \Gamma^h \times \Gamma^h \times \Gamma^h|}$ discretises $\mathbf{M}_{q,j} \in \mathcal{T}^2(\mathbb{R}^2)$, for $j = 1, \dots, Q$;
- $\Psi^{Q,h} = (\Psi_1^{Q,h}, \dots, \Psi_{2^Q}^{Q,h}) \in \mathbb{R}^{|\Gamma^h \times \dots \times \Gamma^h|}$ discretises the test functions $\Psi \in \mathcal{T}^Q(\mathbb{R}^2)$;
- $\mathbf{z}^h = (\mathbf{z}_0^h, \dots, \mathbf{z}_{Q-1}^h)$ discretises the primal variables \mathbf{z} , with $\mathbf{z}_0^h = \mathbf{u}^h \in \mathbb{R}^{|\Omega^h|}$, $\mathbf{z}_0^{\diamond,h} = \mathbf{u}^{\diamond,h}$ and each $\mathbf{z}_j^h \in \mathbb{R}^{|\times_{1,\dots,1}^{j,h} \times \dots \times \times_{2,\dots,2}^{j,h}|}$, for $j = 1, \dots, Q-1$;
- $\mathbf{w}^h = (\mathbf{w}_{q,j}^h)_{q,j}$ discretises the dual variables \mathbf{w} , with each $\mathbf{w}_{q,j}^h \in \mathbb{R}^{|\times_{1,\dots,1}^{j,h} \times \dots \times \times_{2,\dots,2}^{j,h}|}$ for $q = 1, \dots, Q-1$ and $j = 1, \dots, q$; $\mathbf{w}_{Q,j}^h \in \mathbb{R}^{|\Gamma^h \times \dots \times \Gamma^h|}$ for $j = 1, \dots, Q$.

3.3. Isotropic differential operators. Here we discuss the discretization of the adjoint unweighted operators ∇ and div . For $\mathbf{u}^h \in \mathbb{R}^{|\Omega^h|}$, the *discrete gradient* operator is defined as

$$\begin{aligned} \nabla^h : \mathbb{R}^{|\Omega^h|} &\rightarrow \mathbb{R}^{|\times_{1,1}^{1,h} \times \times_{2,1}^{1,h}|} \\ \mathbf{u}^h &\mapsto (\partial_1^h \mathbf{u}^h, \partial_2^h \mathbf{u}^h) \end{aligned}$$

where we use the *central second-order finite difference scheme* on the grids $X_1^{1,h}$, $X_2^{1,h}$:

$$(\partial_1^h \mathbf{u}^h)_{i+\frac{1}{2},j} = \begin{cases} \frac{u_{i+1,j}^h - u_{i,j}^h}{2(\frac{h}{2})} & \text{if } i < M, \\ 0 & \text{if } i = M, \end{cases} \quad \text{and} \quad (\partial_2^h \mathbf{u}^h)_{i,j+\frac{1}{2}} = \begin{cases} \frac{u_{i,j+1}^h - u_{i,j}^h}{2(\frac{h}{2})} & \text{if } j < N, \\ 0 & \text{if } j = N. \end{cases}$$

Let $\mathbf{p}^h = (\mathbf{p}_1^h, \mathbf{p}_2^h) \in \mathbb{R}^{|\times_{1,1}^{1,h} \times \times_{2,1}^{1,h}|}$ and let the *discrete divergence* operator

$$\begin{aligned} \text{div}^h : \mathbb{R}^{|\times_{1,1}^{1,h} \times \times_{2,1}^{1,h}|} &\rightarrow \mathbb{R}^{|\Omega^h|} \\ \mathbf{p}^h &\mapsto \nabla^h \cdot \mathbf{p}^h, \end{aligned}$$

be defined for each pixel (i, j) via the *central second-order difference scheme* on Ω^h :

$$(\operatorname{div}^h \mathbf{p}^h)_{i,j} = \begin{cases} \frac{(\mathbf{p}_1^h)_{i+\frac{1}{2},j}}{2 \left(\frac{h}{2}\right)} & \text{if } i = 1, \\ \frac{(\mathbf{p}_1^h)_{i+\frac{1}{2},j} - (\mathbf{p}_1^h)_{i-\frac{1}{2},j}}{2 \left(\frac{h}{2}\right)} & \text{if } i \in (1, M) + \\ -\frac{(\mathbf{p}_1^h)_{i-\frac{1}{2},j}}{2 \left(\frac{h}{2}\right)} & \text{if } i = M, \end{cases} + \begin{cases} \frac{(\mathbf{p}_2^h)_{i,j+\frac{1}{2}}}{2 \left(\frac{h}{2}\right)} & \text{if } j = 1, \\ \frac{(\mathbf{p}_2^h)_{i,j+\frac{1}{2}} - (\mathbf{p}_2^h)_{i,j-\frac{1}{2}}}{2 \left(\frac{h}{2}\right)} & \text{if } j \in (1, N), \\ -\frac{(\mathbf{p}_2^h)_{i,j-\frac{1}{2}}}{2 \left(\frac{h}{2}\right)} & \text{if } j = N. \end{cases}$$

Thus, the isotropic *discrete gradient* and *discrete divergence* are designed to fulfil the discrete adjointness property, for every $\mathbf{u}^h \in \mathbb{R}^{|\Omega^h|}$ and $\mathbf{p}^h \in \mathbb{R}^{|\mathbb{X}_1^{1,h} \times \mathbb{X}_2^{1,h}|}$:

$$(24) \quad \langle \nabla^h \mathbf{u}^h, \mathbf{p}^h \rangle = - \sum_{(i,j) \in \Omega^h} u_{i,j}^h (\operatorname{div}^h \mathbf{p}^h)_{i,j},$$

where $\langle \cdot, \cdot \rangle : \mathbb{R}^{|\mathbb{X}_1^{1,h} \times \mathbb{X}_2^{1,h}|} \times \mathbb{R}^{|\mathbb{X}_1^{1,h} \times \mathbb{X}_2^{1,h}|} \rightarrow \mathbb{R}$.

For higher-order derivatives of order Q we denote the isotropic *discrete gradient* and *discrete divergence* operator by $\nabla^{Q,h}$ and $\operatorname{div}^{Q,h}$ and write

$$\nabla^{Q,h} : \mathbb{R}^{|\Omega^h|} \rightarrow \mathbb{R}^{|\mathbb{X}_{1,\dots,1}^{Q,h} \times \dots \times \mathbb{X}_{\iota_1, \dots, \iota_Q}^{Q,h} \times \dots \times \mathbb{X}_{2,\dots,2}^{Q,h}|}$$

$$\mathbf{u}^h \mapsto \left(\partial_1^h (\partial_1^h (\dots (\partial_1^h \mathbf{u}^h))), \dots, \partial_{\iota_1}^h (\partial_{\iota_2}^h \dots (\partial_{\iota_q}^h \mathbf{u}^h)), \dots, \partial_2^h (\partial_2^h (\dots \partial_2^h \mathbf{u}^h)) \right)$$

and

$$\operatorname{div}^{Q,h} : \mathbb{R}^{|\mathbb{X}_{1,\dots,1}^{Q,h} \times \dots \times \mathbb{X}_{2,\dots,2}^{Q,h}|} \rightarrow \mathbb{R}^{|\Omega^h|}$$

$$\mathbf{p}^h \mapsto \nabla^{Q,h} \cdot \mathbf{p}^h.$$

The adjointness property is fulfilled for every $\mathbf{u}^h \in \mathbb{R}^{|\Omega^h|}$ and $\mathbf{p}^h \in \mathbb{R}^{|\mathbb{X}_{1,\dots,1}^{Q,h} \times \dots \times \mathbb{X}_{2,\dots,2}^{Q,h}|}$:

$$(25) \quad \langle \nabla^{Q,h} \mathbf{u}^h, \mathbf{p}^h \rangle = - \sum_{(i,j) \in \Omega^h} u_{i,j}^h (\operatorname{div}^{Q,h} \mathbf{p}^h)_{i,j},$$

where $\langle \cdot, \cdot \rangle : \mathbb{R}^{|\mathbb{X}_{1,\dots,1}^{Q,h} \times \dots \times \mathbb{X}_{2,\dots,2}^{Q,h}|} \times \mathbb{R}^{|\mathbb{X}_{1,\dots,1}^{Q,h} \times \dots \times \mathbb{X}_{2,\dots,2}^{Q,h}|} \rightarrow \mathbb{R}$.

3.4. Transfer operators. The mismatched location between \mathbf{z}_0^h , $\nabla^{1,h} \mathbf{z}_0^h$, \dots , $\nabla^{Q,h} \mathbf{z}_0^h$ and the fields \mathcal{M}_q^h associated to \mathbf{v}^h requires the introduction of the following transfer operators, so as to make the quantities computable in the same location. Let $\mathcal{W} := (\mathcal{W}^j)_{j=1}^Q$ be a family of transfer operators $\mathcal{W}^j = (W_\iota^j)$, with $W_\iota^j : \mathbb{R}^{|\mathbb{X}_\iota^{j,h}|} \rightarrow \mathbb{R}^{|\Gamma^h|}$ and ι a multi-index. In practice, \mathcal{W}^j interpolates the data from the grids of j -th order derivatives $\mathbb{X}_\iota^{j,h}$ to the grid of cell centres Γ^h , for W_ι^j averaging operator with partition of unit weights. Its inverse operation is denoted by $(\mathcal{W}^j)^{-1}$.

Example 3.1. For $\mathbf{z}_0^h \in \mathbb{R}^{|\Omega^h|}$ and Q fixed the derivatives are

$$\begin{aligned} \mathbf{w}_{Q,1}^h &:= \nabla^{1,h} \mathbf{z}_0^h = (\partial_1^h \mathbf{z}_0^h, \partial_2^h \mathbf{z}_0^h) \in \mathbb{R}^{|\mathbb{X}_1^{1,h} \times \mathbb{X}_2^{1,h}|}; \\ \mathbf{w}_{Q,2}^h &:= \nabla^{2,h} \mathbf{z}_0^h = (\partial_1^h \partial_1^h \mathbf{z}_0^h, \partial_1^h \partial_2^h \mathbf{z}_0^h, \partial_2^h \partial_1^h \mathbf{z}_0^h, \partial_2^h \partial_2^h \mathbf{z}_0^h) \in \mathbb{R}^{|\mathbb{X}_{1,1}^{2,h} \times \mathbb{X}_{1,2}^{2,h} \times \mathbb{X}_{2,1}^{2,h} \times \mathbb{X}_{2,2}^{2,h}|}; \\ &\vdots \\ \mathbf{w}_{Q,Q}^h &:= \nabla^{Q,h} \mathbf{z}_0^h = (\partial_1^h \dots \partial_1^h \mathbf{z}_0^h, \dots, \partial_2^h \dots \partial_2^h \mathbf{z}_0^h) \in \mathbb{R}^{|\mathbb{X}_{1,\dots,1}^{Q,h} \times \dots \times \mathbb{X}_{2,\dots,2}^{Q,h}|}, \end{aligned}$$

and the transfer operators $\mathcal{W} = (\mathcal{W}^j)_{j=1}^Q$ are

$$\mathcal{W}^j := \begin{cases} \mathcal{W}_{1,\dots,1}^j : \mathbb{R}^{|\mathbb{X}_{1,\dots,1}^{j,h}|} \rightarrow \mathbb{R}^{|\Gamma^h|}, \\ \vdots \\ \mathcal{W}_{\ell_1,\dots,\ell_j}^j : \mathbb{R}^{|\mathbb{X}_{\ell_1,\dots,\ell_j}^{j,h}|} \rightarrow \mathbb{R}^{|\Gamma^h|}, \\ \vdots \\ \mathcal{W}_{2,\dots,2}^j : \mathbb{R}^{|\mathbb{X}_{2,\dots,2}^{j,h}|} \rightarrow \mathbb{R}^{|\Gamma^h|}. \end{cases}$$

Remark 3.2. The choice of the staggered grid increases the accuracy of the solution and allows to compute the inner products between gradients and the vector fields onto a unique regular Cartesian grid of reference, avoiding misplacements. The transfer operators \mathcal{W} reduce the bandwidth of higher order finite difference matrices, improving the quality of the result and reducing the smoothing due to large stencils.

We report in [Figure 3](#) the positions of $\nabla^{Q,h}$, up to order $Q = 3$, in order to visually show how transfer operators \mathcal{W} work for transferring the data on Γ^h .

3.5. Anisotropic differential operators. By construction, $\mathbf{M}_1^h \in \mathbb{R}^{|\Gamma^h \times \Gamma^h| \times |\Gamma^h \times \Gamma^h|}$, when $\mathbf{M}_1^h \neq \mathbf{I}$, but $\nabla^{1,h} \mathbf{u}^h \in \mathbb{R}^{|\mathbb{X}_1^{1,h} \times \mathbb{X}_2^{1,h}|}$, with $\mathbb{R}^{|\mathbb{X}_1^{1,h}|} \neq \mathbb{R}^{|\mathbb{X}_2^{1,h}|} \neq \mathbb{R}^{|\Gamma^h|}$. In this case, locations of $\nabla^{1,h} \mathbf{u}^h$ and \mathbf{M}_1^h are matched via the transfer operators $\mathcal{W}^1 = (\mathcal{W}_1^1, \mathcal{W}_2^1)$.

From [Remark 2.9](#), $\mathbf{M}_1 \nabla \otimes u$ can be discretised in the correct grid position by the operator

$$\mathbf{M}_1^h \mathcal{W}^1 \nabla^{1,h} : \mathbb{R}^{|\Omega^h|} \rightarrow \mathbb{R}^{|\Gamma^h \times \Gamma^h|}$$

and the discretisation reads as

$$\mathbf{M}_1^h \mathcal{W}^1 \nabla^{1,h} \otimes \mathbf{u}^h = \begin{pmatrix} \mathbf{b}_1^h \mathcal{W}_1^1 \nabla^{1,h} \mathbf{u}^h \cdot \mathbf{v}^h \\ \mathbf{b}_2^h \mathcal{W}_2^1 \nabla^{1,h} \mathbf{u}^h \cdot \mathbf{v}_\perp^h \end{pmatrix} = \begin{pmatrix} \mathbf{b}_1^h (\mathcal{W}_1^1 \partial_1^h \mathbf{u}^h \mathbf{v}_1^h + \mathcal{W}_2^1 \partial_2^h \mathbf{u}^h \mathbf{v}_2^h) \\ \mathbf{b}_2^h (\mathcal{W}_2^1 \partial_2^h \mathbf{u}^h \mathbf{v}_1^h - \mathcal{W}_1^1 \partial_1^h \mathbf{u}^h \mathbf{v}_2^h) \end{pmatrix}.$$

Therefore, the discrete weighted divergence $\text{div}_{\mathbf{M}_1^h, \mathcal{W}^1}^h \mathbf{p}^h : \mathbb{R}^{|\Gamma^h \times \Gamma^h|} \rightarrow \mathbb{R}^{|\Omega^h|}$ is

$$(26) \quad \text{div}_{\mathbf{M}_1^h, \mathcal{W}^1}^h \mathbf{p}^h = \nabla^{1,h} \cdot \begin{pmatrix} (\mathcal{W}_1^1)^\top (\mathbf{b}_1^h \mathbf{p}_1^h \mathbf{v}_1^h - \mathbf{b}_2^h \mathbf{p}_2^h \mathbf{v}_2^h) \\ (\mathcal{W}_2^1)^\top (\mathbf{b}_1^h \mathbf{p}_1^h \mathbf{v}_2^h + \mathbf{b}_2^h \mathbf{p}_2^h \mathbf{v}_1^h) \end{pmatrix}.$$

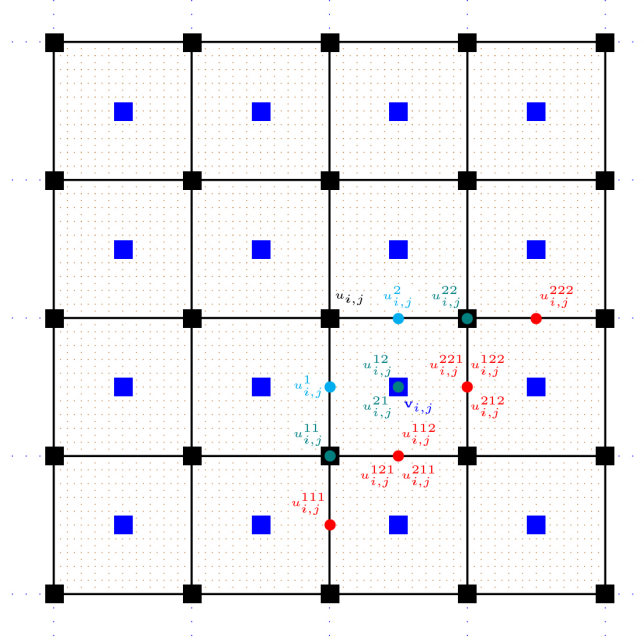


Figure 3: Staggered Grids. We denote $\mathbf{u}^h \in \mathbb{R}^{|\Omega^h|}$ in \blacksquare and $\mathbf{v}^h \in \mathbb{R}^{|\Gamma^h|}$ in \blacksquare . Derivatives of \mathbf{u}^h are denoted by superscripts and located on bullets: $\nabla \mathbf{u}^h = (\partial_1 \mathbf{u}^h, \partial_2 \mathbf{u}^h) = (\mathbf{u}^1, \mathbf{u}^2)$ in \bullet , $\nabla^2 \mathbf{u}^h = (\partial_1 \partial_1 \mathbf{u}^h, \partial_2 \partial_1 \mathbf{u}^h, \partial_1 \partial_2 \mathbf{u}^h, \partial_2 \partial_2 \mathbf{u}^h) = (\mathbf{u}^{11}, \mathbf{u}^{12}, \mathbf{u}^{21}, \mathbf{u}^{22})$ in \bullet and $\nabla^3 \mathbf{u}^h = (\partial_1 \partial_1 \partial_1 \mathbf{u}^h, \dots, \partial_2 \partial_2 \partial_2 \mathbf{u}^h) = (\mathbf{u}^{111}, \dots, \mathbf{u}^{222})$ in \bullet . The transfer operators interpolate values from the (i, j) bullets to the blue (i, j) squares and vice-versa.

This leads to the discrete adjointness property, for every $\mathbf{u}^h \in \mathbb{R}^{|\Omega^h|}, \mathbf{p}^h \in \mathbb{R}^{|\Gamma^h \times \Gamma^h|}$:

$$(27) \quad \langle \mathbf{M}_1^h \mathcal{W}^1 \nabla^{1,h} \mathbf{u}^h, \mathbf{p}^h \rangle = - \sum_{(i,j) \in \Omega^h} u_{i,j}^h (\operatorname{div}_{\mathbf{M}_1^h, \mathcal{W}^1}^h \mathbf{p}^h)_{i,j},$$

where $\langle \cdot, \cdot \rangle : \mathbb{R}^{|\Gamma^h \times \Gamma^h|} \times \mathbb{R}^{|\Gamma^h \times \Gamma^h|} \rightarrow \mathbb{R}$.

When considering higher order derivatives for a generic order Q , the adjoint formula (27) is slightly more complicated due to the recursive definition of the weighted gradient and the location of the nested multiplication.

For a fixed Q we have $\nabla_{\mathcal{M}_Q}^Q u := \mathbf{M}_{Q,Q} \nabla \otimes \dots \otimes \mathbf{M}_{Q,1} \nabla \otimes u$ by Definition 2.10, whose finite-dimensional approximation is $\nabla_{\mathcal{M}_Q^h, \mathcal{W}}^{Q,h} \mathbf{u}^h : \mathbb{R}^{|\Omega^h|} \rightarrow \mathbb{R}^{|\Gamma^h \times \dots \times \Gamma^h|}$, with the recursion

$$(28) \quad \nabla_{\mathcal{M}_Q^h, \mathcal{W}}^{j,h} \mathbf{u}^h := \begin{cases} \mathbf{u}^h & \text{if } j = 0, \\ (\mathcal{W}^j)^T \mathbf{M}_{Q,j}^h \mathcal{W}^j \nabla^h \otimes \nabla_{\mathcal{M}_Q^h, \mathcal{W}}^{j-1,h} \mathbf{u}^h & \text{if } j = 1, \dots, Q-1, \\ \mathbf{M}_{Q,Q}^h \mathcal{W}^Q \nabla^h \otimes \nabla_{\mathcal{M}_Q^h, \mathcal{W}}^{Q-1,h} \mathbf{u}^h & \text{if } j = Q. \end{cases}$$

Note that in (28) for $q = Q$ we omitted the inverse transfer operator $(\mathcal{W}^Q)^T$ since unnecessary,

so as to keep $\nabla_{\mathcal{M}_Q^h, \mathcal{W}}^{\mathcal{Q}, h} \mathbf{u}^h \in \mathbb{R}^{|\Gamma^h \times \dots \times \Gamma^h|}$ and match with the position of $\Psi^{\mathcal{Q}, h}$.

Also, $\text{div}_{\mathcal{M}_Q^h, \mathcal{W}}^{\mathcal{Q}, h} : \mathbb{R}^{|\Gamma^h \times \dots \times \Gamma^h|} \rightarrow \mathbb{R}^{|\Omega^h|}$ is the finite-dimensional approximation of $\text{div}_{\mathcal{M}_Q}^{\mathcal{Q}}$, with the recursion

$$(29) \quad \text{div}_{\mathcal{M}_Q^h, \mathcal{W}}^{j, h} \Psi^{\mathcal{Q}, h} := \begin{cases} \Psi^{\mathcal{Q}, h} & \text{if } j = 0, \\ \nabla^h \cdot (\mathbf{M}_{Q, Q}^h \mathcal{W}^{\mathcal{Q}})^T \Psi^{\mathcal{Q}, h} & \text{if } j = 1, \\ \nabla^h \cdot (\mathbf{M}_{Q, Q-j+1}^h \mathcal{W}^{\mathcal{Q}-j+1})^T \mathcal{W}^{\mathcal{Q}-j+1} \text{div}_{\mathcal{M}_Q^h, \mathcal{W}}^{j-1, h} \Psi^{\mathcal{Q}, h} & \text{if } 2 < j \leq \mathcal{Q}. \end{cases}$$

For every $\mathbf{u}^h \in \mathbb{R}^{|\Omega^h|}$, $\mathbf{p}^h \in \mathbb{R}^{|\Gamma^h \times \dots \times \Gamma^h|}$, the discrete adjointness property holds:

$$(30) \quad \langle \nabla_{\mathcal{M}_Q^h, \mathcal{W}}^{\mathcal{Q}, h} \mathbf{u}^h, \mathbf{p}^h \rangle = (-1)^{\mathcal{Q}} \sum_{(i, j) \in \Omega^h} u_{i, j}^h (\text{div}_{\mathcal{M}_Q^h, \mathcal{W}}^{\mathcal{Q}, h} \mathbf{p}^h)_{i, j},$$

where $\langle \cdot, \cdot \rangle : \mathbb{R}^{|\Gamma^h \times \dots \times \Gamma^h|} \times \mathbb{R}^{|\Gamma^h \times \dots \times \Gamma^h|} \rightarrow \mathbb{R}$.

4. Numerical optimisation. In what follows, we solve (16) by a primal-dual hybrid gradient method [15, 16]. With all discrete objects in place, we define the discretization of the joint TDV $_{\alpha}^{\mathcal{Q}} - L^2$ problem (16) following [11, Equation 4.4] as:

$$\min_{\mathbf{z}_0^h \in \mathbb{R}^{|\Omega^h|}} \sum_{q=1}^{\mathcal{Q}} \text{TDV}_{\alpha_q}^{q, h}(\mathbf{z}_0^h, \mathcal{M}_q^h) + \frac{\eta}{2} \left\| \mathcal{S} \mathbf{z}_0^h - \mathbf{z}_0^{\diamond, h} \right\|_2^2,$$

where the discrete version of TDV $_{\alpha}^q$ is

$$\text{TDV}_{\alpha_q}^{q, h}(\mathbf{z}_0^h, \mathcal{M}_q^h) = \sup_{\Psi^{q, h} \in \mathcal{Y}_{\mathcal{M}_q^h, \alpha}^{q, h}} \langle \mathbf{z}_0^h, \text{div}_{\mathcal{M}_q^h, \mathcal{W}}^{q, h} \Psi^{q, h} \rangle$$

and $\mathbf{z}_0^{\diamond, h} = \mathbf{u}^{\diamond, h} \in \mathbb{R}^{|\Omega^h|}$, \mathcal{S} is the operator associated to the problem to solve, $\text{div}_{\mathcal{M}_q^h, \mathcal{W}}^{q, h}$ is the discretized weighted divergence, with respect to the weights \mathcal{M}_q^h and the transfer operators in \mathcal{W} , $\mathcal{Y}_{\mathcal{M}_q^h, \alpha}^{q, h}$ is the discretization of $\mathcal{Y}_{\mathcal{M}_q, \alpha}^q$ from (21), defined as

$$(31) \quad \mathcal{Y}_{\mathcal{M}_q^h, \alpha}^{q, h} = \left\{ \Psi^{q, h} \in \mathbb{R}^{2q|\Gamma^h|} \mid \left\| \text{div}_{\mathcal{M}_q^h, \mathcal{W}}^{j, h} \Psi^{q, h} \right\|_{\infty} \leq \alpha_j, \text{ for all } j = 1, \dots, q-1 \right\}.$$

4.1. Operator norm. Following the approach in [11, Section 4] and [15, Section 6.1], we estimate a bound on the norm of the linear operator $\nabla_{\mathcal{M}_q^h, \mathcal{W}}^{q, h}$ in (28) in view of the implementation of a suitable primal-dual algorithm. For each $q = 1, \dots, \mathcal{Q}$, we have

$$(32) \quad L_q^2 = \left\| \nabla_{\mathcal{M}_q^h, \mathcal{W}}^{q, h} \right\|^2 = \left\| \text{div}_{\mathcal{M}_q^h, \mathcal{W}}^{q, h} \right\|^2 = \sup_{\Psi^h \in \mathcal{Y}_{\mathcal{M}_q^h, \alpha}^{q, h}} \frac{\left\| \text{div}_{\mathcal{M}_q^h, \mathcal{W}}^{q, h} \Psi^h \right\|^2}{\left\| \Psi^h \right\|^2}.$$

In the two-dimensional setting, when $q = 1$ then $\text{div}_{\mathcal{M}_1^h, \mathcal{W}}^{1, h} \Psi^h$ in (32) reduces to

$$\text{div}_{\mathcal{M}_1^h, \mathcal{W}}^{1, h} \Psi^h = \text{div}^{1, h} ((\mathbf{M}_{1,1}^h \mathcal{W}^1)^T \Psi^h)$$

and by applying the finite difference scheme in (26), from $\|\nabla\| \leq \sqrt{8}h^{-1}$, we estimate:

$$\begin{aligned} L_1^2 &= \left\| \operatorname{div}_{\mathcal{M}_1^h, \mathcal{W}}^{1,h} \Psi^h \right\|^2 = \operatorname{div}_{\mathcal{M}_1^h, \mathcal{W}}^{1,h} \Psi^h \cdot \operatorname{div}_{\mathcal{M}_1^h, \mathcal{W}}^{1,h} \Psi^h \\ &= \operatorname{div}((\mathbf{M}_{1,1}^h \mathcal{W}^1)^T \Psi^h) \cdot \operatorname{div}((\mathbf{M}_{1,1}^h \mathcal{W}^1)^T \Psi^h) \\ &= \mathbf{M}_{1,1}^h \mathcal{W}^1 \nabla \otimes \operatorname{div} \left((\mathbf{M}_{1,1}^h \mathcal{W}^1)^T \Psi^h \right) \cdot \Psi^h \leq \frac{8}{h^2} \left\| \mathbf{M}_{1,1}^h \mathcal{W}^1 \right\|_F^2 \left\| \Psi^h \right\|^2. \end{aligned}$$

For a fixed Q , since it holds

$$\left\| (\mathcal{W}^j)^T \mathbf{M}_{Q,j}^h \mathcal{W}^j \right\|_F = \left\| ((\mathcal{W}^j)^T \mathbf{M}_{Q,j}^h \mathcal{W}^j)^T \right\|_F, \quad \text{for each } j = 1, \dots, Q,$$

then the operator norm L_Q is estimated via

$$(33) \quad L_Q^2 \leq (8h^{-2})^Q \prod_{j=1}^Q \left\| (\mathcal{W}^j)^T \mathbf{M}_{Q,j}^h \mathcal{W}^j \right\|_2^2.$$

Remark 4.1. Since \mathcal{W} is made by partition of unit transfer operators and $\left\| \mathbf{M}_{Q,j}^h \right\|_2 \leq 1$ by construction, we can estimate the right-hand side of (33) as:

$$L_Q^2 \leq (8h^{-2})^Q.$$

which agrees with the classic isotropic setting given by the choices $\mathbf{M}_{Q,j}^h = \mathbf{I}$ without the use of \mathcal{W}^j for every $j = 1, \dots, Q$. Indeed, we have $L^2 \leq 8h^{-2}$ for TV and $L^2 \leq 64h^{-4}$ for $\operatorname{TGV}_\alpha^2$.

4.2. Discrete characterisation of TDV. For a fixed $q = 1, \dots, Q$, the regulariser $\operatorname{TDV}_\alpha^{q,h}$ can be characterised as follows. From the discrete version of $\operatorname{TGV}_\alpha^q$ in [45, Section 4.1] and following the characterization of $\operatorname{TGV}_\alpha^q$ in [11, Remark 3.8 and Remark 3.10], we can write the equivalent discrete definition of $\operatorname{TDV}_\alpha^q(u, \mathcal{M})$ for $\mathbf{u}^h \in \mathbb{R}^{|\Omega^h|}$ and $\mathcal{M}^h = (\mathcal{M}_j^h)_{j=1}^q$ as

$$(34) \quad \operatorname{TDV}_\alpha^{q,h}(\mathbf{u}^h, \mathcal{M}^h) = \inf_{\substack{\mathbf{z}_j^h \in \mathbb{R}^{|\mathcal{X}_i^{j,h}|} \\ j=0, \dots, q, \\ \mathbf{z}_0 = \mathbf{u}^h, \mathbf{z}_q = \mathbf{0}}} \sum_{j=1}^q \alpha_{q-j} \left\| (\mathcal{K}_q^h)_{j,j} \mathbf{z}_{j-1}^h - \mathbf{z}_j^h \right\|_{2,1},$$

with

$$(35) \quad (\mathcal{K}_q^h)_{j,j} = \begin{cases} (\mathcal{W}^j)^T \mathbf{M}_j^h \mathcal{W}^j \nabla^h & \text{if } j = 1, \dots, q-1, \\ \mathbf{M}_q^h \mathcal{W}^q \nabla^h & \text{if } j = q. \end{cases}$$

Indeed, in the following let $j = 1, \dots, q$, $\mathbf{w}_{q-j+1}^h \in \mathbb{R}^{|\mathcal{X}_i^{q-j+1}|}$ and $\mathbf{z}_{q-j}^h \in \mathbb{R}^{|\mathcal{X}_i^{q-j,h}|}$. We call

$$\operatorname{DV}_\alpha^{j,h}(\mathbf{w}_{q-j+1}^h, \mathcal{M}^h) = \sup_{\Psi^h \in \mathcal{J}_{\mathcal{M}^h, \alpha}^{q,h}} -\langle (\mathcal{W}^{q-j+1})^T \mathbf{M}_{q-j+1}^h \mathcal{W}^{q-j+1} \mathbf{w}_{q-j+1}^h, \operatorname{div}_{\mathcal{M}^h, \mathcal{W}}^{j-1} \Psi^h \rangle$$

where $\operatorname{div}_{\mathcal{M}^h, \mathcal{W}}^{j-1}$ as in (29) and $\mathcal{Y}_{\mathcal{M}^h, \alpha}^{q,h}$ as in (31). Note that the sup is finite since we are in finite dimension. Thus $\operatorname{TDV}_{\alpha}^{q,h}(\mathbf{u}^h, \mathcal{M}^h) = \operatorname{DV}_{\alpha}^{q,h}(\nabla^h \mathbf{u}^h, \mathcal{M}^h)$ and we define

$$K_{\ell}^h = \left\{ \Psi^h : \Psi^h \in \mathcal{Y}_{\mathcal{M}^h, \alpha}^{j,h}, \left\| \operatorname{div}_{\mathcal{M}^h, \mathcal{W}}^{\ell,h} \Psi \right\|_{\infty} \leq \alpha_{\ell} \right\} \quad \text{for every } \ell = 0, \dots, q-1.$$

With $\mathbf{s}_{q,j}^h = \mathbf{M}_q^h \mathcal{W}^q \nabla^h \otimes \dots \otimes (\mathcal{W}^{q-j+2})^T \mathbf{M}_{q-j+2}^h \mathcal{W}^{q-j+2} \nabla^h$ and $(j-1)$ -times integration by parts, the functional becomes

$$\operatorname{DV}_{\alpha}^{j,h}(\mathbf{w}_{q-j+1}^h, \mathcal{M}^h) = \left(\sum_{\ell=0}^{j-1} \delta_{K_{\ell}^h} \right)^* \left((-1)^j \mathbf{s}_{q,j}^h \otimes (\mathcal{W}^{q-j+1})^T \mathbf{M}_{q-j+1}^h \mathcal{W}^{q-j+1} \mathbf{w}_{q-j+1}^h \right).$$

By Fenchel duality for the operator $\operatorname{div}_{\mathcal{M}^h, \mathcal{W}}^{j-1,h}$ we have:

$$\begin{aligned} \operatorname{DV}_{\alpha}^{j,h}(\nabla^h \mathbf{z}_{q-j}^h, \mathcal{M}^h) &= \sup_{\Psi^h} \left(\begin{aligned} & -\langle (\mathcal{W}^{q-j+1})^T \mathbf{M}_{q-j+1}^h \mathcal{W}^{q-j+1} \nabla^h \mathbf{z}_{q-j}^h, \operatorname{div}_{\mathcal{M}^h, \mathcal{W}}^{j-1,h} \Psi \rangle \\ & - \delta_{K_{j-1}^h}(\Psi^h) - \sum_{\ell=0}^{j-2} \delta_{K_{\ell}^h}(\Psi^h) \end{aligned} \right) \\ &= \sup_{\Psi^h} \left(\begin{aligned} & - \sum_{\ell=0}^{j-2} \delta_{K_{\ell}^h}(\Psi) - \delta_{\{\|\cdot\| \leq \alpha_{j-1}\}}(\operatorname{div}_{\mathcal{M}^h, \mathcal{W}}^{j-1,h} \Psi^h) \\ & - \langle (\mathcal{W}^{q-j+1})^T \mathbf{M}_{q-j+1}^h \mathcal{W}^{q-j+1} \mathbf{z}_{q-j}^h, \operatorname{div}_{\mathcal{M}^h, \mathcal{W}}^{j-1,h} \Psi^h \rangle \end{aligned} \right) \\ &= \inf_{\mathbf{z}_{q-j+1}^h} \left(\begin{aligned} & \alpha_{j-1} \left\| (\mathcal{W}^{q-j+1})^T \mathbf{M}_{q-j+1}^h \mathcal{W}^{q-j+1} \nabla^h \mathbf{z}_{q-j}^h - \mathbf{z}_{q-j+1}^h \right\|_1 \\ & + \left(\sum_{\ell=0}^{j-2} \delta_{K_{\ell}^h} \right)^* \left((-1)^{j-1} \mathbf{s}_{q,j+1}^h \mathbf{z}_{q-j+1}^h \right) \end{aligned} \right) \\ &= \inf_{\mathbf{z}_{q-j+1}^h} \left(\begin{aligned} & \alpha_{j-1} \left\| (\mathcal{W}^{q-j+1})^T \mathbf{M}_{q-j+1}^h \mathcal{W}^{q-j+1} \nabla^h \mathbf{z}_{q-j}^h - \mathbf{z}_{q-j+1}^h \right\|_1 \\ & + \operatorname{DV}_{\alpha}^{j-1,h}(\nabla^h \mathbf{z}_{q-j+1}^h, \mathcal{M}^h) \end{aligned} \right). \end{aligned}$$

Iterating the procedure for $j = q, \dots, 2$ and by the identity

$$\operatorname{DV}_{\alpha}^{1,h}(\nabla^h \mathbf{z}_{q-1}^h) = \alpha_0 \left\| \mathbf{M}_q^h \mathcal{W}^q \nabla^h \mathbf{z}_{q-1}^h \right\|_1,$$

we get

$$\operatorname{DV}_{\alpha}^{q,h}(\nabla^h \mathbf{z}_0^h) = \inf_{\substack{\mathbf{z}_j^h \in \mathbb{R}^{|\mathcal{X}_j^h|} \\ j=1, \dots, q-1 \\ \mathbf{z}_0^h = \mathbf{u}^h}} \left(\sum_{j=1}^{q-1} \alpha_{q-j} \left\| \mathcal{W}^j \mathbf{M}_j^h \mathcal{W}^j \nabla^h \mathbf{z}_{j-1}^h - \mathbf{z}_j^h \right\|_1 \right) + \alpha_0 \left\| \mathbf{M}_q^h \mathcal{W}^q \nabla^h \mathbf{z}_{q-1}^h \right\|_1$$

and thus, with $(\mathcal{K}_q^h)_{j,j}$ as in (35), we conclude

$$\operatorname{TDV}_{\alpha}^{q,h}(\mathbf{u}^h, \mathcal{M}^h) = \inf_{\substack{\mathbf{z}_j^h \in \mathbb{R}^{|\mathcal{X}_j^h|} \\ j=1, \dots, q \\ \mathbf{z}_0^h = \mathbf{u}^h, \mathbf{z}_q^h = \mathbf{0}}} \left(\sum_{j=1}^q \alpha_{q-j} \left\| (\mathcal{K}_q^h)_{j,j} \mathbf{z}_{j-1}^h - \mathbf{z}_j^h \right\|_1 \right).$$

A continuous version of (34) also holds. This is proved in the second part of this work [39].

The characterisation of $\text{TDV}_\alpha^{q,h}$ in (34) is fundamental for writing a suitable primal-dual algorithm for the minimization problem in (16).

4.3. Discretised single minimization problem. Let u^\diamond be given imaging data. For a fixed order $Q = 1, 2, 3$, let $\text{TDV}_\alpha^{Q,h}$ be as in (34) and $\mathcal{M}_Q^h = (\mathbf{M}_{Q,j}^h)_{j=1}^Q$ be the collection of discrete tensor fields. Thus, we have the following discrete single minimization problems from (16):

- for order $Q = 1$, $\mathcal{M}_1^h = \mathbf{M}_{1,1}^h$, $\alpha = \alpha_{1,0}$, $\mathbf{z}^h = \mathbf{z}_0^h$:

$$(36) \quad \min_{\mathbf{z}^h} \alpha_{1,0} \left\| (\mathcal{W}^1)^\top \mathbf{M}_{1,1}^h \mathcal{W}^1 \nabla^h \mathbf{z}_0^h \right\|_{2,1} + \frac{\eta}{2} \left\| \mathcal{S} \mathbf{z}_0^h - \mathbf{z}_0^{\diamond,h} \right\|_2^2;$$

- for order $Q = 2$, $\mathcal{M}_2^h = (\mathbf{M}_{2,1}^h, \mathbf{M}_{2,2}^h)$, $\alpha = (\alpha_{2,0}, \alpha_{2,1})$, $\mathbf{z}^h = (\mathbf{z}_0^h, \mathbf{z}_1^h)$:

$$(37) \quad \min_{\mathbf{z}^h} \left(\begin{array}{l} \alpha_{2,1} \left\| (\mathcal{W}^1)^\top \mathbf{M}_{2,1}^h \mathcal{W}^1 \nabla^h \mathbf{z}_0^h - \mathbf{z}_1^h \right\|_{2,1} \\ + \alpha_{2,0} \left\| (\mathcal{W}^2)^\top \mathbf{M}_{2,2}^h \mathcal{W}^2 \nabla^h \mathbf{z}_1^h \right\|_{2,1} + \frac{\eta}{2} \left\| \mathcal{S} \mathbf{z}_0^h - \mathbf{z}_0^{\diamond,h} \right\|_2^2 \end{array} \right);$$

- for order $Q = 3$, $\mathcal{M}_3^h = (\mathbf{M}_{3,1}^h, \mathbf{M}_{3,2}^h, \mathbf{M}_{3,3}^h)$, $\alpha = (\alpha_{3,0}, \alpha_{3,1}, \alpha_{3,2})$, $\mathbf{z}^h = (\mathbf{z}_0^h, \mathbf{z}_1^h, \mathbf{z}_2^h)$:

$$(38) \quad \min_{\mathbf{z}^h} \left(\begin{array}{l} \alpha_{3,2} \left\| (\mathcal{W}^1)^\top \mathbf{M}_{3,1}^h \mathcal{W}^1 \nabla^h \mathbf{z}_0^h - \mathbf{z}_1^h \right\|_{2,1} \\ + \alpha_{3,1} \left\| (\mathcal{W}^2)^\top \mathbf{M}_{3,2}^h \mathcal{W}^2 \nabla^h \mathbf{z}_1^h - \mathbf{z}_2^h \right\|_{2,1} \\ + \alpha_{3,0} \left\| (\mathcal{W}^3)^\top \mathbf{M}_{3,3}^h \mathcal{W}^3 \nabla^h \mathbf{z}_2^h \right\|_{2,1} + \frac{\eta}{2} \left\| \mathcal{S} \mathbf{z}_0^h - \mathbf{z}_0^{\diamond,h} \right\|_2^2 \end{array} \right).$$

4.4. Discretised joint minimization problem. A single-line combination of (36)–(38) leads to the discretisation of the joint saddle-point minimisation problem:

$$(39) \quad \mathbf{u}^* \in \arg \min_{\mathbf{u}^h \in \mathbb{R}^{|\Omega^h|}} \sum_{q=1}^Q \text{TDV}_{\alpha_q}^{q,h}(\mathbf{u}^h, \mathcal{M}_q^h) + \frac{\eta}{2} \left\| \mathcal{S} \mathbf{u}^h - \mathbf{u}^{\diamond,h} \right\|_2^2.$$

We aim to provide a more concise formulation of (39). Let \mathbf{z}^h be as above, $\mathcal{M}_q^h = (\mathcal{M}_q^h)_{q=1}^Q$ be a family of collections of tensor fields and $\mathcal{K}^h = (\mathcal{K}_q^h)_{q=1}^Q$ be a collection of operators where, for a fixed regularisation order q , each $\mathcal{M}_q^h = (\mathcal{M}_{q,j}^h)_{j=1}^q$ is a collection of tensor fields and each \mathcal{K}_q^h is the associated operator defined as

$$(40) \quad \mathcal{K}_q^h = \begin{pmatrix} (\mathcal{K}_q^h)_{1,1} & -\mathbf{I} & \mathbf{0} & \dots & \dots & \dots & \mathbf{0} \\ \mathbf{0} & (\mathcal{K}_q^h)_{2,2} & -\mathbf{I} & \mathbf{0} & & & \vdots \\ \vdots & \ddots & \ddots & \ddots & \ddots & & \vdots \\ \vdots & & \mathbf{0} & (\mathcal{K}_q^h)_{j,j} & -\mathbf{I} & \mathbf{0} & \vdots \\ \vdots & & & \ddots & \ddots & \ddots & \mathbf{0} \\ \vdots & & & & \mathbf{0} & (\mathcal{K}_q^h)_{q-1,q-1} & -\mathbf{I} \\ \mathbf{0} & \dots & \dots & \dots & \dots & \mathbf{0} & (\mathcal{K}_q^h)_{q,q} \end{pmatrix},$$

with $(\mathcal{K}_q^h)_{j,\ell} = \mathbf{0}$ if $\ell \neq \{j, j+1\}$, $(\mathcal{K}_q^h)_{j,j+1} = -\mathbf{I}$ and

$$(\mathcal{K}_q^h)_{j,j} = \begin{cases} (\mathcal{W}^j)^\top \mathbf{M}_{q,j}^h \mathcal{W}^j \nabla^h & \text{if } j = 1, \dots, q-1, \\ \mathbf{M}_{q,q}^h \mathcal{W}^q \nabla^h & \text{if } j = q. \end{cases}$$

Let \mathbf{A} be the weight matrix, with $\mathbf{a} = \text{diag}(\mathbf{A})$ and in each q -th column the q -th order weights:

$$(41) \quad \mathbf{A} = \begin{pmatrix} \alpha_{1,0} & \alpha_{2,1} & \alpha_{3,2} & \dots & \alpha_{q,q-1} & \dots & \dots & \alpha_{Q,Q-1} \\ 0 & \alpha_{2,0} & \alpha_{3,1} & \dots & \alpha_{q,q-2} & \dots & \dots & \alpha_{Q,Q-2} \\ \vdots & 0 & \alpha_{3,0} & \dots & \alpha_{q,q-3} & \dots & \dots & \alpha_{Q,Q-3} \\ \vdots & & 0 & \ddots & \vdots & & & \vdots \\ \vdots & & & \ddots & \alpha_{q,0} & & & \alpha_{Q,Q-q} \\ \vdots & & & & 0 & \ddots & & \vdots \\ \vdots & & & & & \ddots & \ddots & \vdots \\ 0 & \dots & \dots & \dots & \dots & \dots & 0 & \alpha_{Q,0} \end{pmatrix}.$$

Example 4.2. For $Q = 3$, the Equation (42) has the following entries:

$$\mathbf{A} = \begin{pmatrix} \alpha_{1,0} & \alpha_{2,1} & \alpha_{3,2} \\ 0 & \alpha_{2,0} & \alpha_{3,1} \\ 0 & 0 & \alpha_{3,0} \end{pmatrix}, \quad \begin{aligned} \mathcal{M}_1^h &= (\mathbf{M}_{1,1}^h), \\ \mathcal{M}_2^h &= (\mathbf{M}_{2,1}^h, \mathbf{M}_{2,1}^h), \\ \mathcal{M}_3^h &= (\mathbf{M}_{3,1}^h, \mathbf{M}_{3,2}^h, \mathbf{M}_{3,3}^h), \end{aligned}$$

$$\mathcal{K}_1^h = \begin{pmatrix} \mathbf{M}_{1,1}^h \mathcal{W}^1 \nabla^h & \mathbf{0} & \mathbf{0} \\ \mathbf{0} & \mathbf{0} & \mathbf{0} \\ \mathbf{0} & \mathbf{0} & \mathbf{0} \end{pmatrix}, \quad \mathcal{K}_2^h = \begin{pmatrix} (\mathcal{W}^1)^\top \mathbf{M}_{2,1}^h \mathcal{W}^1 \nabla^h & -\mathbf{I} & \mathbf{0} \\ \mathbf{0} & \mathbf{M}_{2,2}^h \mathcal{W}^2 \nabla^h & \mathbf{0} \\ \mathbf{0} & \mathbf{0} & \mathbf{0} \end{pmatrix},$$

$$\mathcal{K}_3^h = \begin{pmatrix} (\mathcal{W}^1)^\top \mathbf{M}_{3,1}^h \mathcal{W}^1 \nabla^h & -\mathbf{I} & \mathbf{0} \\ \mathbf{0} & (\mathcal{W}^2)^\top \mathbf{M}_{3,2}^h \mathcal{W}^2 \nabla^h & -\mathbf{I} \\ \mathbf{0} & \mathbf{0} & \mathbf{M}_{3,3}^h \mathcal{W}^3 \nabla^h \end{pmatrix}.$$

Thus, solving (39) is equivalent to solve for $\mathbf{z}^h = (\mathbf{z}_0^h, \dots, \mathbf{z}_{Q-1}^h)$ the following problem:

$$(42) \quad \mathbf{u}^* \in \arg \min_{\mathbf{u}^h \in \mathbb{R}^{|\Omega^h|}} \inf_{\mathbf{z}^h} \sum_{q=1}^Q \sum_{j=1}^q \mathbf{A}_{j,q} \left\| \sum_{\ell=1}^q (\mathcal{K}_q^h)_{j,\ell} \mathbf{z}_{\ell-1}^h \right\|_{2,1} + \frac{\eta}{2} \left\| \mathcal{S} \mathbf{u}^h - \mathbf{u}^{\otimes, h} \right\|_2^2.$$

By duality of $\|\cdot\|_{2,1}$ norm, let $\mathbf{w}^h = (\mathbf{w}_{q,j}^h)_{q,j}$ be the dual vector for $q = 1, \dots, Q$ and $j = 1, \dots, q$ with $\mathbf{w}_{q,j}^h \in \mathbb{R}^{|\mathbb{X}_{1,\dots,1}^{j,h} \times \dots \times \mathbb{X}_{2,\dots,2}^{j,h}|}$. Thus, we rewrite (42) into a joint saddle-point minimization problem:

$$(43) \quad \min_{\mathbf{z}^h} \max_{\mathbf{w}^h} \sum_{q=1}^Q \left(\left\langle \sum_{\ell=1}^q (\mathcal{K}_q^h)_{j,\ell} \mathbf{z}_{\ell-1}^h, \mathbf{w}_{q,j}^h \right\rangle - \sum_{j=1}^q \delta_{\{\|\cdot\|_{2,\infty} \leq \mathbf{A}_{j,q}\}}(\mathbf{w}_{q,j}^h) \right) + \frac{\eta}{2} \left\| \mathcal{S} \mathbf{z}_0^h - \mathbf{z}_0^{\otimes, h} \right\|_2^2,$$

or, in short notation:

$$(44) \quad \min_{\mathbf{z}^h} \max_{\mathbf{w}^h} \langle \mathcal{K}^h \mathbf{z}^h, \mathbf{w}^h \rangle - F^*(\mathbf{w}^h) + G(\mathbf{z}_0^h),$$

with

$$F^*(\mathbf{w}^h) = \sum_{q=1}^Q \sum_{j=1}^q \delta_{\{\|\cdot\|_{2,\infty} \leq \mathbf{A}_{j,q}\}}(\mathbf{w}_{q,j}^h), \quad G(\mathbf{z}_0^h) = \frac{\eta}{2} \left\| \mathcal{S} \mathbf{z}_0^h - \mathbf{z}_0^{\diamond,h} \right\|_2^2.$$

4.5. Proximal operators. We want to solve the saddle point problem (44) with a primal-dual algorithm, which requires the computation of the proximal operators of F^* and G .

The proximal map of F^* at \mathbf{w}^h is the sum of the projections onto the respective polar balls since F^* is fully separable:

$$\mathbf{prox}_{\sigma F^*}(\mathbf{w}^h) = \sum_{q=1}^Q \sum_{j=1}^q \mathbf{prox}_{\sigma F^*}(\mathbf{w}_{q,j}^h), \quad \text{with} \quad \mathbf{prox}_{\sigma F^*}(\mathbf{w}_{q,j}^h) = \frac{\mathbf{w}_{q,j}^h}{\max\left(1, \mathbf{A}_{j,q}^{-1} \|\mathbf{w}_{q,j}^h\|_2\right)}.$$

The proximal map of G at $\hat{\mathbf{u}}^h \in \mathbb{R}^{|\Omega^h|}$ is:

$$\mathbf{prox}_{\tau G}(\hat{\mathbf{u}}^h) = \arg \min_{\mathbf{u}^h \in \mathbb{R}^{|\Omega^h|}} \frac{\eta}{2} \left\| \mathcal{S} \mathbf{u}^h - \mathbf{u}^{\diamond,h} \right\|_2^2 + \frac{1}{2\tau} \left\| \mathbf{u}^h - \hat{\mathbf{u}}^h \right\|_2^2,$$

whose minimum is achieved by a \mathbf{u}^h that solves, for \mathcal{S}^* adjoint of \mathcal{S} ,

$$\begin{aligned} \tau \eta \mathcal{S}^*(\mathcal{S} \mathbf{u}^h - \mathbf{u}^{\diamond,h}) + (\mathbf{u}^h - \hat{\mathbf{u}}^h) &= 0 \\ (\mathbf{I} + \tau \eta \mathcal{S}^* \mathcal{S}) \mathbf{u}^h - \tau \eta \mathcal{S}^* \mathbf{u}^{\diamond,h} - \hat{\mathbf{u}}^h &= 0 \\ (\mathbf{I} + \tau \eta \mathcal{S}^* \mathcal{S}) \mathbf{u}^h - \tau \eta \mathcal{S}^* \mathbf{u}^{\diamond,h} - \hat{\mathbf{u}}^h + \tau \eta \mathcal{S}^* \mathcal{S} \hat{\mathbf{u}}^h - \tau \eta \mathcal{S}^* \mathcal{S} \hat{\mathbf{u}}^h &= 0 \\ (\mathbf{I} + \tau \eta \mathcal{S}^* \mathcal{S})(\mathbf{u}^h - \hat{\mathbf{u}}^h) &= \tau \eta \mathcal{S}^*(\mathbf{u}^{\diamond,h} - \mathcal{S} \hat{\mathbf{u}}^h). \end{aligned}$$

Thus, we get $\mathbf{u}^h = \mathbf{prox}_{\tau G}(\hat{\mathbf{u}}^h) = \hat{\mathbf{u}}^h + (\mathbf{I} + \tau \eta \mathcal{S}^* \mathcal{S})^{-1} \tau \eta \mathcal{S}^*(\mathbf{u}^{\diamond,h} - \mathcal{S} \hat{\mathbf{u}}^h)$.

Note that for the Rudin-Osher-Fatemi problem we have $\mathcal{S} = \mathbf{I}$, thus $\mathcal{S}^* = \mathbf{I}$, and the proximal map agrees with the one computed in [15, pag. 133].

4.6. Primal-dual algorithm. Now we are ready for solving (44) to formulate the primal-dual algorithm [15]. Let $L = \|\mathcal{K}\|$ the operator norm, i.e. $L := \sup_{\mathbf{z}} \{\|\mathcal{K} \mathbf{z}\| \text{ s.t. } \|\mathbf{z}\|_2 \leq 1\}$, and let $\tau, \sigma > 0, \omega \in [0, 1]$, such that $\tau \sigma L^2 \leq 1$. When acceleration is possible, an adaptive strategy for τ, σ and ω can be used: let L_G be the Lipschitz constant of G , $\tau_0 = L^{-1}$, $\sigma_0 \tau_0 L^2 = 1$ and $\gamma = 0.5 L_G^{-1}$. We denote by a superscript n the iterations of the primal-dual algorithm. Then, starting from admissible $\mathbf{z}^{0,h}$ and $\mathbf{w}^{0,h}$, we iterate

$$(45) \quad \begin{aligned} \mathbf{w}^{n+1,h} &= \mathbf{prox}_{\sigma_n F^*} \left(\mathbf{w}^{n,h} + \sigma_n \mathcal{K}^h \bar{\mathbf{z}}^{n,h} \right); \\ \mathbf{z}^{n+1,h} &= \mathbf{prox}_{\tau_n G} \left(\mathbf{z}^{n,h} - \tau_n (\mathcal{K}^h)^* \mathbf{w}^{n+1,h} \right); \\ \omega_n &= (1 + 2\gamma \tau_n)^{-0.5}; \tau_{n+1} = \omega_n \tau_n; \sigma_{n+1} = \sigma_n \omega_n^{-1}; \\ \bar{\mathbf{z}}^{n+1,h} &= \mathbf{z}^{n+1,h} + \omega_n (\mathbf{z}^{n+1,h} - \mathbf{z}^{n,h}). \end{aligned}$$

The final solution is found by $\mathbf{u}^h = \mathbf{z}_0^{n+1,h}$. Compare Algorithm 1 for details.

Algorithm 1 Primal-dual algorithm for the joint minimization model in Equation (44)

Parameters for the model : $Q > 0$ and $\eta > 0$.

Operators needed : \mathcal{K}^h and \mathbf{A} (e.g. as in Example 4.2).

Parameters for primal-dual: $\sigma_0, \tau_0, \omega_0, L = \|\mathcal{K}^h\|$ such that $\sigma_0\tau_0L^2 \leq 1; \gamma > 0$.

Initialization : $\mathbf{z}^{0,h} := (\mathbf{z}_{j-1}^{0,h}), \mathbf{z}_0^{0,h} = \mathbf{u}^{\diamond,h}, \mathbf{w}^{0,h} = (\mathbf{w}_{q,j}^{0,h})$ for $q, j = 1, \dots, Q$.

Function PrimalDual($\mathbf{u}^{\diamond,h}, \mathcal{K}^h, \mathbf{A}, \eta$):

```

while stopping criterion is not satisfied do
  for  $q = 1, \dots, Q$  do
    for  $j = 1, \dots, q - 1$  do
       $\mathbf{w}_{q,j}^{n,h} = \mathbf{w}_{q,j}^{n,h} + \sigma_n \left( (\mathcal{K}_{q,h})_{j,j} \bar{\mathbf{z}}_{j-1}^{n,h} - \bar{\mathbf{z}}_j^{n,h} \right);$  // Update the dual
       $\mathbf{w}_{q,j}^{n+1,h} = \mathbf{w}_{q,j}^{n,h} / \max \left( 1, \mathbf{A}_{j,q}^{-1} \|\mathbf{w}_{q,j}^{n,h}\|_2 \right);$  // Proximal operator of  $F^*$ 
    end
     $\mathbf{w}_{q,q}^{n,h} = \mathbf{w}_{q,q}^{n,h} + \sigma_n (\mathcal{K}_q^h)_{q,q} \bar{\mathbf{z}}_{q-1}^{n,h};$ 
     $\mathbf{w}_{q,q}^{n+1,h} = \mathbf{w}_{q,q}^{n,h} / \max \left( 1, \mathbf{A}_{q,q}^{-1} \|\mathbf{w}_{q,q}^{n,h}\|_2 \right);$ 
  end
  for  $j = 2, \dots, Q$  do
     $\mathbf{z}_{j-1}^{n,h} = \mathbf{z}_{j-1}^{n,h} - \tau_n \sum_{q=1}^Q \left( (\mathcal{K}_q^h)^*_{j,j} \mathbf{w}_{q,j}^{n+1,h} - \mathbf{w}_{q,j-1}^{n+1,h} \right);$  // Update the primal
  end
   $\mathbf{z}_0^{n,h} = \mathbf{z}_0^{n,h} - \tau_n \sum_{q=1}^Q \left( (\mathcal{K}_q^h)^*_{1,1} \mathbf{w}_{q,1}^{n+1,h} \right);$ 
   $\mathbf{z}_0^{n+1,h} = \mathbf{z}_0^{n,h} + (\mathbf{I} + \tau\eta\mathcal{S}^*\mathcal{S})^{-1}\tau\eta\mathcal{S}^*(\mathbf{z}_0^{\diamond,h} - \mathcal{S}\mathbf{z}_0^{n,h});$  // Proximal operator of  $G$ 
   $\omega_n = (1 + 2\gamma\tau_n)^{-0.5}; \tau_{n+1} = \omega_n\tau_n; \sigma_{n+1} = \sigma_n\omega_n^{-1};$  // Update  $\omega_n, \tau_n, \sigma_n$ 
   $\bar{\mathbf{z}}^{n+1,h} = \mathbf{z}^{n+1,h} + \omega_n(\mathbf{z}^{n+1,h} - \mathbf{z}^{n,h});$  // Extrapolation step
end
return  $\mathbf{u}^* = \mathbf{z}_0^{n+1,h}$ .

```

Remark 4.3. If $\mathcal{S} = \mathbf{I}$, then the fidelity term G is uniformly convex, with convexity parameter η , so acceleration is possible, e.g. [15, Algorithm 2], since the dual problem is smooth. When G is not strongly convex, the use of [15, Algorithm 1] is recommended since the resulting dual problem is non-smooth, e.g. when \mathcal{S} is a projection map onto a subset.

5. Imaging applications. In what follows we demonstrate the performance of the introduced total directional regulariser TDV_{α}^Q for the applications of image denoising, image zooming and surface interpolation. We in particular focus on the cases $Q = 1, 2, 3$ and $\alpha = 1$.

5.1. Image Denoising. Let $\Omega \subset \mathbb{R}^2$, $u : \Omega \rightarrow \mathbb{R}$ be a grey-scale image, $\mathbf{v} : \Omega \rightarrow \mathbb{R}^2$ be a unitary vector field and u^{\diamond} be a given noisy image. For colour images $\mathbf{u} : \Omega \rightarrow \mathbb{R}^3$ we consider

one colour channel at time. We consider (16) for $Q = 3$, each \mathcal{M}_q^a for $q = 1, 2, 3$ as in (23) with $a = 1$ and $\mathcal{S} = \mathbf{I}$:

$$(46) \quad u^* \in \arg \min_u \sum_{q=1}^Q \text{TDV}_{\alpha_q}^q(u, \mathcal{M}_q^1) + \frac{\eta}{2} \|u - u^\diamond\|_2^2.$$

In the following, we will require that $\mathbf{b} = (1, b_2(\mathbf{x}))^\top$ for every $\mathbf{x} \in \Omega$ such that

$$\mathbf{M} \nabla \otimes u = \mathbf{\Lambda}_b(\mathbf{R}_\theta)^\top \nabla \otimes u = \begin{pmatrix} \nabla_{\mathbf{v}} u \\ b_2(\mathbf{x}) \nabla_{\mathbf{v}_\perp} u \end{pmatrix},$$

where \mathbf{v} is a given estimated field. Letting the primal vector $\mathbf{z} = (z_0, z_1, z_2)$, $z_0 = u$, we solve the minimization problem (46) using the equivalent formulation (42), with:

$$(47) \quad \mathbf{A} = \begin{pmatrix} \alpha_{1,0} & +\infty & +\infty \\ 0 & \alpha_{2,0} & +\infty \\ 0 & 0 & \alpha_{3,0} \end{pmatrix}, \quad \begin{aligned} \mathcal{M}_1 &= (\mathbf{M}), \\ \mathcal{M}_2 &= (\mathbf{I}, \mathbf{M}), \\ \mathcal{M}_3 &= (\mathbf{I}, \mathbf{I}, \mathbf{M}), \end{aligned} \quad \mathbf{a} = \text{diag}(\mathbf{A}) = (\alpha_{1,0}, \alpha_{2,0}, \alpha_{3,0}),$$

$$(48) \quad \mathcal{K}_1 = \begin{pmatrix} \mathbf{M}\mathcal{W}^1 \nabla & \mathbf{0} & \mathbf{0} \\ \mathbf{0} & \mathbf{0} & \mathbf{0} \\ \mathbf{0} & \mathbf{0} & \mathbf{0} \end{pmatrix}, \quad \mathcal{K}_2 = \begin{pmatrix} \nabla & -\mathbf{I} & \mathbf{0} \\ \mathbf{0} & \mathbf{M}\mathcal{W}^2 \nabla & \mathbf{0} \\ \mathbf{0} & \mathbf{0} & \mathbf{0} \end{pmatrix}, \quad \mathcal{K}_3 = \begin{pmatrix} \nabla & -\mathbf{I} & \mathbf{0} \\ \mathbf{0} & \nabla & -\mathbf{I} \\ \mathbf{0} & \mathbf{0} & \mathbf{M}\mathcal{W}^3 \nabla \end{pmatrix}.$$

When entry (j, q) of \mathbf{A} is equal to $+\infty$, then we require $\mathbf{z}_j^n = (\mathcal{K}_q)_{j,j} \mathbf{z}_{j-1}$. Thus, with the choices of \mathbf{A} and \mathcal{K} as above, the denoising problem in equation (46) can be simplified as

$$(49) \quad u^* \in \arg \min_u \left(\begin{aligned} &\alpha_{1,0} \|\mathbf{M}\mathcal{W}^1 \nabla u\|_{2,1} + \alpha_{2,0} \|\mathbf{M}\mathcal{W}^2 \nabla^2 u\|_{2,1} + \alpha_{3,0} \|\mathbf{M}\mathcal{W}^3 \nabla^3 u\|_{2,1} \\ &+ \frac{\eta}{2} \|u - u^\diamond\|_2^2 \end{aligned} \right),$$

and solved via the primal-dual [Algorithm 1](#).

Estimation of vector field \mathbf{v} . For estimating \mathbf{v} we use the following strategy. Let $\sigma, \rho > 0$. Let $\lambda_1(\mathbf{x}), \lambda_2(\mathbf{x})$ be such that $\lambda_1(\mathbf{x}) \geq \lambda_2(\mathbf{x})$, the ordered eigenvalues of

$$(50) \quad \mathbf{J}_\rho(u) := K_\rho * (\nabla u_\sigma \otimes \nabla u_\sigma) \quad \text{for } u_\sigma := K_\sigma * u,$$

and $\mathbf{e}_1, \mathbf{e}_2 \in \mathbb{R}^2$ the associated eigenvectors. Let $\tilde{\mathbf{v}}(\mathbf{x}) = \mathbf{e}_2(\mathbf{x})$ be the local direction of the anisotropy, corresponding to an approximation of $(\nabla^\perp u) / \|\nabla^\perp u\|$. In order to compute a vector field smoother than $\tilde{\mathbf{v}}$, we adopt a further regularisation step, similarly as in [31].

Let $w(\mathbf{x}) \in [0, 1]$. We aim to smooth the vector field where the anisotropy weight $w(\mathbf{x})$ is close to 0 while keeping the already computed vector field in regions with strong anisotropy. This is equivalent to solving the following problem:

$$(51) \quad \mathbf{v} = \arg \min_{\mathbf{z}} \frac{1}{2} \int_{\Omega} w(\mathbf{x}) \|\mathbf{z}(\mathbf{x}) - \tilde{\mathbf{v}}(\mathbf{x})\|_2^2 \, d\mathbf{x} + \frac{\gamma}{2} \int_{\Omega} \|\nabla \tilde{\mathbf{v}}(\mathbf{x})\|_2^2 \, d\mathbf{x}.$$

We use the local estimation of the anisotropy as weights $w(\mathbf{x})$, for $\varepsilon > 0$:

$$(52) \quad w(\mathbf{x}) = \frac{\lambda_1(\mathbf{x}) - \lambda_2(\mathbf{x})}{\lambda_1(\mathbf{x}) + \lambda_2(\mathbf{x}) + \varepsilon}.$$

We can use $w(\mathbf{x})$ also to vary locally $\mathbf{b} = (1, b_2(\mathbf{x}))$: we have already seen that $b_2(\mathbf{x})$ close to 1 results in an isotropic process while $b_2(\mathbf{x})$ close to 0 results in a fully anisotropic process. For this reason, a possible strategy to vary $b_2(\mathbf{x})$ is:

- firstly estimate the anisotropy (values close to 1 correspond to isotropic regions) by:

$$(53) \quad b_2(\mathbf{x}) = 1 - w(\mathbf{x}),$$

- secondly rescale $b_2(\mathbf{x})$ in $[0, 1]$ via

$$(54) \quad b_2(\mathbf{x}) = \frac{b_2(\mathbf{x}) - \min b_2(\mathbf{x})}{\max b_2(\mathbf{x}) - \min b_2(\mathbf{x})}.$$

With this strategy, the higher the image anisotropy the closer \mathbf{b} is to $(1, 0)$: in such cases strong directional structures are emphasised by $\text{TDV}_{\alpha}^{\text{Q}}(u, \mathcal{M})$. Conversely, when $\mathbf{b} = (1, 1)$, isotropic smoothing is performed in flat regions. We may also refine \mathbf{v} by updating the parameters (σ, ρ) so as to restart the denoising problem with a better estimation of the vector field. The computation for u and \mathbf{v} are performed alternately as described in [Algorithm 2](#).

Algorithm 2 Iterative scheme of the discrete denoising problem in [\(49\)](#)

Parameters for the model : $\mathbf{a} = (\alpha_{1,0}, \alpha_{2,0}, \alpha_{3,0})$, $\mathbf{b}^h = (\mathbf{I}, \mathbf{b}_2^h)$, $\eta > 0$, $a = 1$.

Parameters for \mathbf{v} : $\sigma_1, \rho_1 > 0$.

Function $\text{TDV_denoising}(\mathbf{u}^{\diamond, h})$:

```

for  $k = 1, \dots, \text{maxiter}$  do
     $[\mathbf{v}^{k+1, h}, \mathbf{b}^{k+1, h}] = \text{compute\_v\_and\_b}(\mathbf{u}^k, \sigma_k, \rho_k)$ ; // from (50)-(54)
     $\mathcal{K}^{k+1, h} = \text{build\_K}(\mathbf{a}, \mathbf{v}^{k+1, h}, \mathbf{b}^{k+1, h})$ ; // update  $\mathcal{K}$ 
     $\mathbf{u}^{k+1, h} = \text{primal\_dual}(\mathbf{u}^{\diamond, h}, \mathcal{K}^{k+1, h}, \mathbf{a}, \eta)$ ; // restart denoising with a better  $\mathbf{v}$ 
     $[\sigma_{k+1}, \rho_{k+1}] = \text{update\_sigmarho}(\sigma_k, \rho_k)$ ; // new structure tensor parameters
end
return  $\mathbf{u}^{k+1, h}$ 

```

Numerical Results. We discuss denoising results obtained with [Algorithm 2](#) for images with strong directional features: [Figure 4](#) shows the performance for a fixed choice of $b_2(\mathbf{x})$, while [Figures 6](#) and [7](#) for varying $b_2(\mathbf{x})$, compared to the non-local method BM3D [\[19\]](#).

Bamboo image. The bamboo image in [Figure 4a](#) has been corrupted by 20% of Gaussian noise using the same random seed as in [\[20\]](#), see [Figure 4b](#). We estimated the vector field \mathbf{v} as described before, with a fixed choice of \mathbf{b} so as to fix the elliptic shape of the test functions. In [Figures 4c](#) and [4d](#), we report the results from [\[20\]](#) related to the use of classic TV and TGV regularisers, where the staircasing effect is visible as expected. The DTV and DTGV approaches from [\[20\]](#), in [Figure 4e](#) and [Figure 4f](#) respectively, seems promising, even

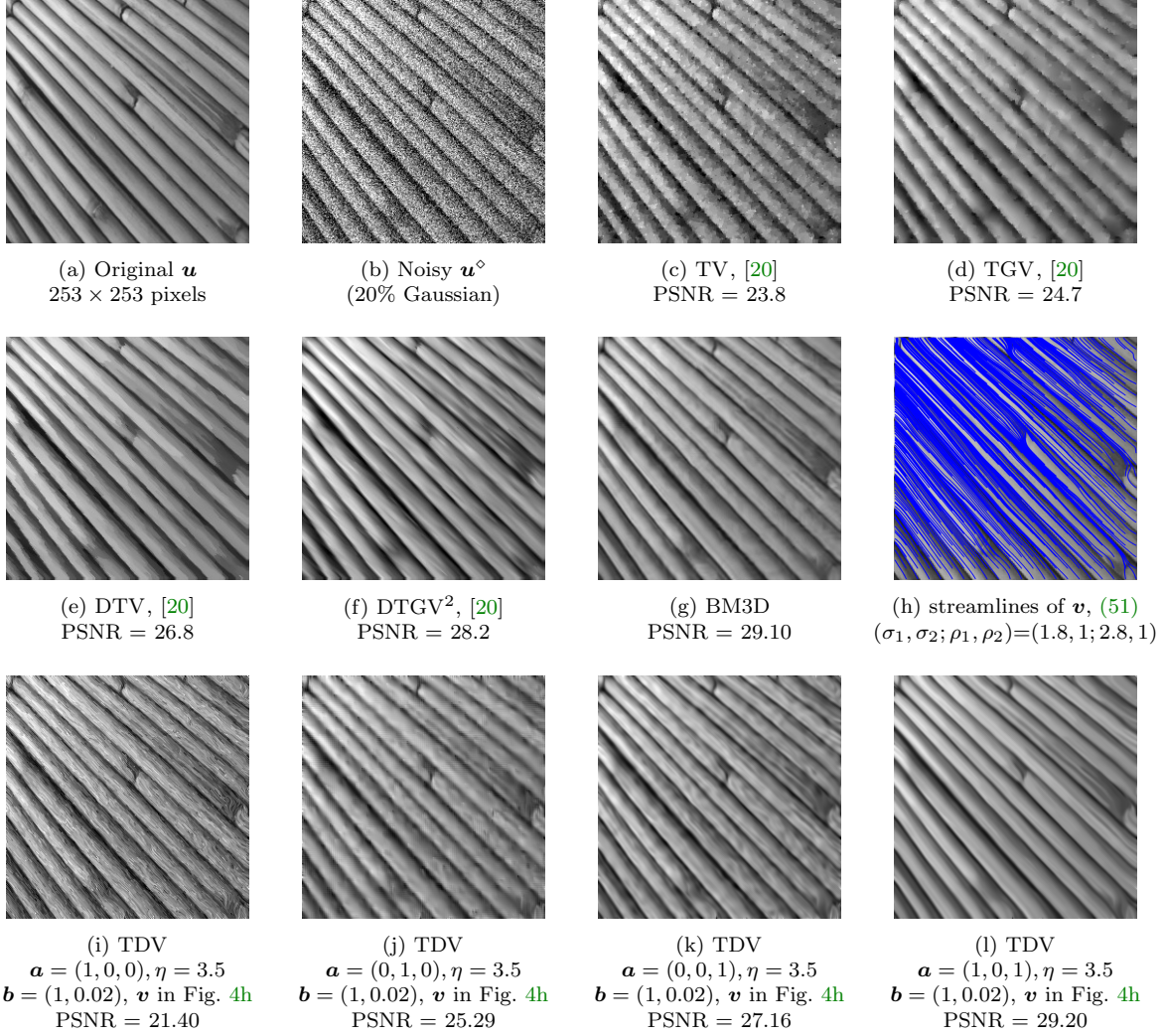


Figure 4: Denoising of bamboo grey-scale image.

if obtained with a single direction only. In our case we consider multiple directions \mathbf{v} , with $\gamma = 2$ in equation (51) and suitable (ρ, σ) in equation (50) to produce \mathbf{v} as in Figure 4h from the noisy data in Figure 4b. Here, we have chosen $\eta = 3.5$ as the optimal parameter for the fidelity term, according to the noise level expected. We run Algorithm 2 for 1000 iterations: we also restarted the algorithm with a better estimation of \mathbf{v} after a first run. We firstly report the single order regularisers results: $Q = 1$ in Figure 4i, $Q = 2$ in Figure 4j and $Q = 3$ in Figure 4k. Moreover, the result from the joint combination of first and third order directional regularisers, TDV_α^1 and TDV_α^3 , is shown in Figure 4l. We omitted results obtained by possible combinations of TDV_α^2 since results were smoother than needed across edges due to the nature of the regulariser involving the weighted Hessian.

For the joint combination TDV_α^1 and TDV_α^3 , namely $\mathbf{a} = (1, 0, 1)$, we report in Figure 5

the PSNR results for different fixed choices of $\mathbf{b} = (1, b_2)$ and of (σ_1, ρ_1) from (50) and (51), with fixed refinement $(\sigma_2, \rho_2) = (1, 1)$, leading to different vector fields \mathbf{v} . We vary (σ_1, ρ_1) in the range between $(1.5, 3.5)$, with $\rho_1 - \sigma_1$ in the $x - y$ axes, for the cases $b_2 = 0$ in Figure 5a, $b_2 = 0.01$ in Figure 5b, $b_2 = 0.02$ in Figure 5c and $b_2 = 0.03$ in Figure 5d.

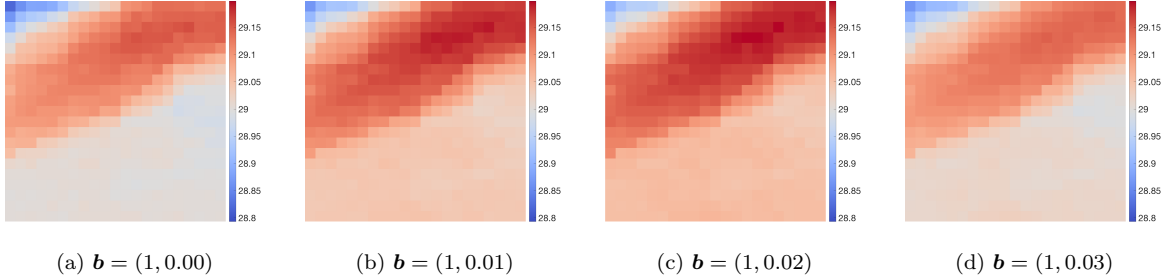


Figure 5: PSNR consistency on Figure 4b with fixed $\mathbf{a} = (1, 0, 1)$, $\eta = 3.5$ and varying \mathbf{b} , (σ, ρ) . On the x-axis, ρ_1 ; on the y-axis σ_1 , with $\sigma_1, \rho_1 \in [1.5, 3.5]$ and fixed $(\sigma_2, \rho_2) = (1, 1)$.

We conclude that a combination of first and third order directional regularisers is a competitor of the nonlocal denoising approach BM3D [19] and it performs better than results obtained in [20]. Also, the robustness of the approach depends on the computation of \mathbf{v} as shown in Figure 5, where minor variations of \mathbf{v} leads to minor variations in the PSNR result.

A natural question now is whether allowing also $b_2(\mathbf{x})$ to change in Ω improves the performances. We are going to answer this question in the next two experiments.

Rainbow. The rainbow in Figure 6a has been corrupted by 20% of Gaussian noise in each color channel, see Figure 6b. Due to the particular structure of the image, an isotropic approach seems reasonable outside the rainbow while an anisotropic approach inside. This resulted in varying the b_2 parameter following equations (53)-(54): in Figure 6d the black pixels corresponds to $b_2 \approx 0$ and the white pixels to $b_2 \approx 1$. Indeed for $b_2 \rightarrow 0$ we expect to denoise the image following the anisotropy induced by \mathbf{v} , while for $b_2 \rightarrow 1$ we expect to denoise the image isotropically in both \mathbf{v} and \mathbf{v}_\perp directions. In order to compute the vector field \mathbf{v} as in Figure 6e, we did not apply the regularisation step (51) and we did not iterate Algorithm 2 since both the resulting \mathbf{v} and \mathbf{b} seem good enough for our purposes, performing better than BM3D in Figure 6c, with less wavy artefacts and a smoother global structure.

Desert. The desert image in Figure 7a is a mix of anisotropic and isotropic information. We denoised Figure 7b, corrupted again with 20% of Gaussian noise in each color channel, with $(\sigma, \rho) = (3, 1.5)$ and $\gamma = 0.1$ to estimate \mathbf{v} in Figure 7e as described before. We also allowed $b_2(\mathbf{x})$ to vary across the domain and we did not refine \mathbf{v} with further iterations. Here, BM3D in Figure 7c performed slightly better than our approach due to the wrong estimation of \mathbf{v} along some dune waves: this is clearly visible in Figures 7d and 7e where both the wrong estimation of \mathbf{v} and the isotropy requirement of b_2 result in a smoothing performance, as shown in the zooms of Figures 7g and 7h. However, we recall that BM3D is a non-local method and better performances than local methods are expected.

5.2. Wavelet Zooming. In this section we apply our regularisation to wavelet-based image zooming as in [10]. Here, the data fidelity term is modelled by a wavelet transformation operator. Let $\phi \in L^2(\mathbb{R})$, $\psi \in L^2(\Omega)$ be the scaling and mother wavelet function, respectively.

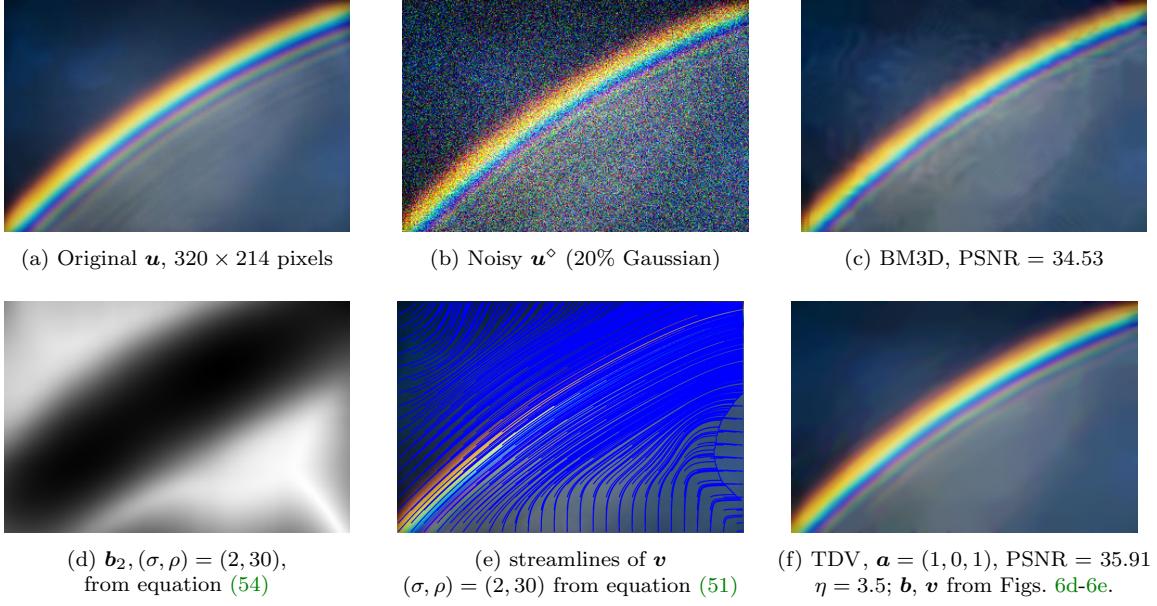


Figure 6: Denoising of RGB rainbow (photo by M.P. Markkanen, CC-BY-SA-4.0 license).

Then, a Riesz' basis of $L^2(\Omega)$ is obtained from translations and rotations of ϕ and ψ . Here, we will consider only functions ϕ with compact support, yielding a compactly supported basis elements. Let $R \in \mathbb{Z}$ be a resolution level and $M_R, (L_j)_{j \leq R}$ be finite index sets in \mathbb{Z}^2 , then:

- a Riesz' basis of $L^2((0, 1) \times (0, 1))$ is $(\phi_{R, \mathbf{k}})_{\mathbf{k} \in M_R}, (\psi_{j, \mathbf{k}})_{j \leq R, \mathbf{k} \in L_j}$;
- the dual basis of the above is defined as $(\tilde{\phi}_{R, \mathbf{k}})_{\mathbf{k} \in M_R}, (\tilde{\psi}_{j, \mathbf{k}})_{j \leq R, \mathbf{k} \in L_j}$.

Thus, the following decomposition holds:

$$u = \sum_{\mathbf{k} \in M_R} (u, \phi_{R, \mathbf{k}})_2 \tilde{\phi}_{R, \mathbf{k}} + \sum_{j \leq R, \mathbf{k} \in L_j} (u, \psi_{j, \mathbf{k}})_2 \tilde{\psi}_{j, \mathbf{k}}.$$

Let $u_0 \in \text{span} \left\{ \tilde{\phi}_{R, \mathbf{k}} \mid \mathbf{k} \in M_R \right\}$ be a low resolution version of u given by $((u_0, \phi_{R, \mathbf{k}})_2)_{\mathbf{k} \in M_R}$, where the unknown u is such that $(u, \phi_{R, \mathbf{k}})_2 = (u_0, \phi_{R, \mathbf{k}})_2$, for all $\mathbf{k} \in M_R$, and

$$u \in L^2(\Omega) = \text{span} \left(\left\{ \tilde{\phi}_{R, \mathbf{k}} \mid \mathbf{k} \in M_R \right\} \cup \left\{ \tilde{\psi}_{j, \mathbf{k}} \mid j \leq R, \mathbf{k} \in L_j \right\} \right).$$

The wavelet-based zooming problem with higher order total directional regularisers reads as

$$u^* \in \arg \min_u \sum_{q=1}^Q \text{TDV}_{\alpha_q}^q(u, \mathcal{M}) + \mathcal{I}_{U_D}(u),$$

where $U_D = \{u \in L^2(\Omega) \mid (u, \phi_{R, \mathbf{k}})_2 = (u_0, \phi_{R, \mathbf{k}})_2, \text{ for all } \mathbf{k} \in M_R\}$, see [10] for more details. Since we did not downsampled the original image, we avoided artefacts introduced by algorithms for reducing the image but at the same time no ground truth is available. Results based on CDF 9/7 wavelet are shown in Figure 8 for grey-scale images and in Figure 9 for color images, with \mathcal{A} and \mathcal{K} defined as in equations (47) and (48).

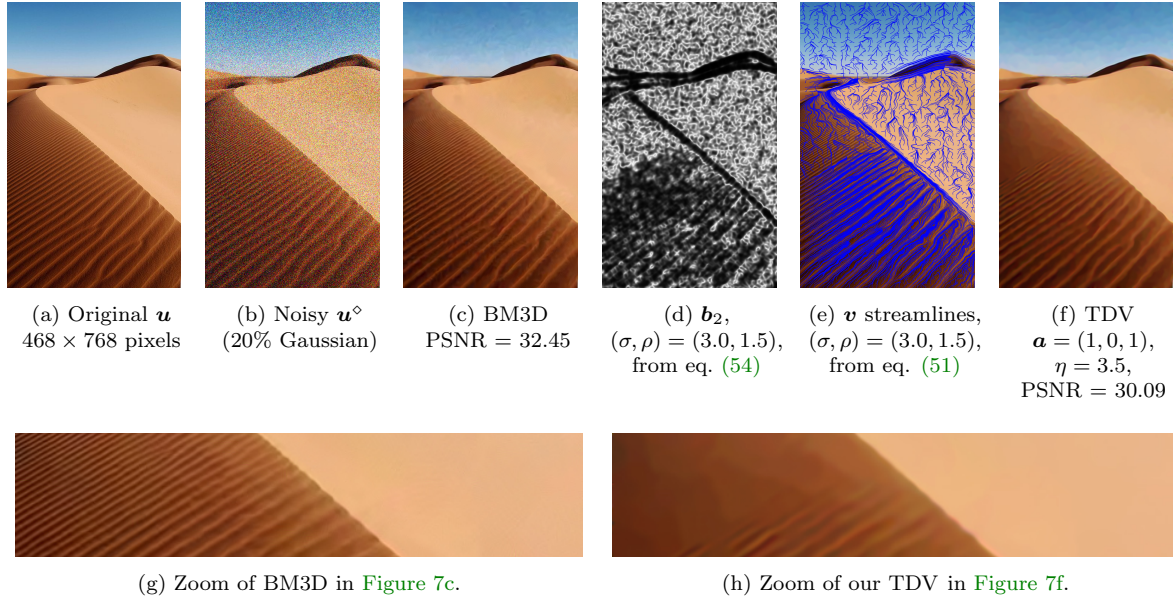


Figure 7: Denoising of RGB desert (photo by Rosino, CC-BY-SA-2.0 license).

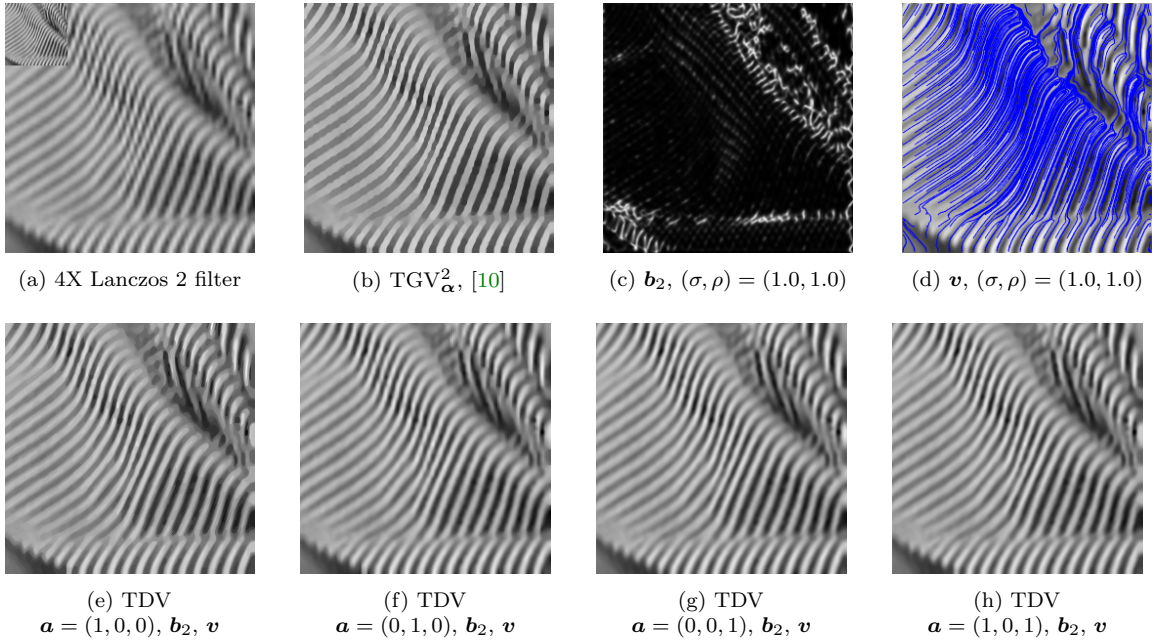


Figure 8: Wavelet-based zooming with CDF 9/7.

5.3. Surface Interpolation. In this experiment, we aim to reconstruct a surface from scattered height data available in Ω . The available data lies on partially occluded isolines or

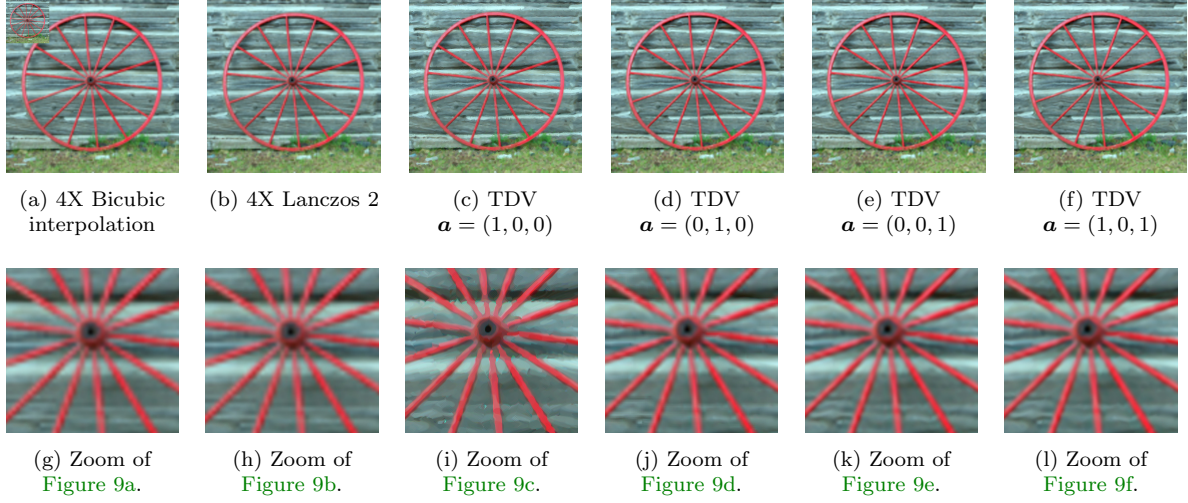


Figure 9: Wavelet-based zooming with CDF 9/7. Image from the MorgueFile archive.

on random points in Ω and the challenge is to interpolate them by preserving the anisotropic features via the reconstruction of a suitable vector field \mathbf{v} . Before presenting our approach for this problem using $\text{TDV}_{\alpha}^{\mathbf{Q}}$, we briefly review the state-of-the-art for surface interpolation.

Related works. The reconstruction of surfaces from scattered height values has been approached in two different ways in the literature: based on explicit and implicit models. Surface interpolation is sometimes also addressed as *digital elevation map* (DEM) problem.

In this paper we focus on implicit surface interpolation which has the advantage of being independent with respect to parametrization. Here the surface is an implicit function of height values over the domain. Two prominent methods in this range are the Thin Plate Spline (TPS) [34] and the *Absolute Minimizing Lipschitz Extension* (AMLE) [2] approach. TPS is a flexible approach since it can embed both grey values and gradient information. However, it has the drawback to be a fourth order isotropic method and the resulting interpolated surface is isotropically smooth. AMLE, on the other hand, is able to interpolate data given in isolated points and on curves but it fails to interpolate slopes of a surface, resulting in C^1 , see [42].

For interpolating surfaces with sharp features, e.g. strong creases, and possibly non-smooth features, e.g. corners in a pyramid, it seems promising therefore to consider (higher-order) total variation (TV) regularisers for surface interpolation.

Our main model approach here is [31], where a third-order directional total variation regulariser has been proposed that reads for a given vector field \mathbf{v} as

$$(55) \quad E(u) = \int_{\Omega} \|\nabla_{\mathbf{v}}(\nabla^2 u)\|_2,$$

where $\nabla_{\mathbf{v}}^3 u = \nabla(\nabla^2 u) \cdot \mathbf{v}$ is the directional derivative of the Hessian of u , along \mathbf{v} . Note that this is a special case of $\text{TDV}_{\alpha}^{\mathbf{Q}}$ with $\mathbf{Q} = 3$, $a = 1$, $\mathbf{b} = (1, 0)$, $\mathbf{v} = (\cos \theta, \sin \theta)$, i.e. $\mathcal{M} = (\mathbf{I}, \mathbf{I}, \mathbf{M})$ and $\mathbf{M} = \Lambda_{\mathbf{b}}(\mathbf{R}_{\theta})^T$, leading to $\nabla_{\mathbf{v}}^3 u \equiv \mathbf{M} \nabla \otimes (\nabla^2 u)$.

The estimation of \mathbf{v} is crucial to obtain a good quality result. In [31], \mathbf{v} has been computed as a two step minimization-regularisation problem by solving firstly

$$\tilde{\mathbf{v}} = \arg \min_{\substack{\mathbf{y} \\ \|\mathbf{y}\|_2=1}} \left\| K_\sigma * \nabla \left(\frac{\nabla u}{|\nabla u|} \right) (\mathbf{x}) \mathbf{y} \right\|_2;$$

and then applying to $\tilde{\mathbf{v}}$ the same regularisation step in (51), where $w(\mathbf{x})$ is a weight chosen as the largest singular value of $K_\sigma * \nabla \left(\frac{\nabla u}{|\nabla u|} \right)$ and ρ is a regularising parameter in order to smooth areas where the surface u is almost planar and to preserve locally the vector field $\tilde{\mathbf{v}}$ in areas where the level lines have large curvature. As last step, \mathbf{v} is normalised to be unitary.

Another directional interpolation model for u and \mathbf{v} appear in [8]: differently from our approach in this paper, it requires knowledge of the vector field \mathbf{v} , a-priori to the interpolation.

In this section, we generalize the approach of [31] for the reconstruction of a surface, given scattered height values lying (possibly) on partial contour lines. Differently from Section 5.1, the unitary vector field \mathbf{v} is reconstructed in the missing domain as follows.

Let Ω a 2D domain ($d = 2$) and u^\diamond sparse sampled height values. In the following, the projection onto the data available u^\diamond is identified by the operator \mathcal{S} . We aim to find the interpolated surface $u : \Omega \rightarrow \mathbb{R}$, driven by the unitary directions $\mathbf{v} : \Omega \rightarrow \mathbb{R}^2$. Let $\mathcal{M}^a = (\mathcal{M}_1^a, \dots, \mathcal{M}_Q^a)$ be a collection of weighting fields, where for a fixed q the collection \mathcal{M}_q^a is defined as in (23) with explicit dependence on \mathbf{v} . We solve by Algorithm 3, alternately:

$$(56) \quad u^* \in \arg \min_u \sum_{q=1}^Q \text{TDV}_{\alpha_q}^q(u, \mathcal{M}_q^a(\mathbf{v})) + \frac{\eta}{2} \|\mathcal{S}u - u^\diamond\|_2^2,$$

$$(57) \quad \mathbf{v}^* \in \arg \min_{\mathbf{v}} \mu \text{TV}(\mathbf{v}) + \zeta \int_{\Omega} \left(1 - \mathbf{v} \cdot \frac{\nabla u}{|\nabla u|} \right)^2 d\mathbf{x},$$

with the primal-dual in Algorithm 1 for (56) and a classic primal-dual for (57). In particular, in (57) we identify $F(\mathbf{v}) = \text{TV}(\mathbf{v})$ for regularising the vector field \mathbf{v} and $G(\mathbf{v}) = \left\| 1 - \mathbf{v} \cdot \frac{\nabla u}{|\nabla u|} \right\|_{L^2}^2$ for normalising \mathbf{v} in the direction of the normalised gradient [4].

Algorithm 3 Alternating scheme for the surface interpolation problem in (56) and (57)

Input : the sparse data u^\diamond in Ω .

Parameters : α_q for $q = 1, \dots, Q$, $a > 0$, $\eta > 0$, $\mu, \zeta > 0$.

Initialization : random u^0 and \mathbf{v}^0 , $\mathcal{S}(u^0) = u^\diamond$, $t = 0$.

Update : u^t and \mathbf{v}^t as follows.

while *stopping criterion is not satisfied* **do**

$$u^{t+1} \in \arg \min_{u \in \mathbb{R}} \sum_{q=1}^Q \text{TDV}_{\alpha_q}^q(u, \mathcal{M}_q^a(\mathbf{v}^t)) + \frac{\eta}{2} \|\mathcal{S}u - u^\diamond\|_2^2; \quad // \text{ Minimization w.r.t. } u$$

$$\mathbf{v}^{t+1} \in \arg \min_{\mathbf{v} \in \mathbb{R}^2} \mu \text{TV}(\mathbf{v}) + \zeta \int_{\Omega} \left(1 - \mathbf{v} \cdot \frac{\nabla u^{t+1}}{|\nabla u^{t+1}|} \right)^2 d\mathbf{x}; \quad // \text{ Minimization w.r.t. } \mathbf{v}$$

Update $\mathcal{M}_q^a(\mathbf{v}^{t+1})$ for each $q = 1, \dots, Q$; // update the weights

end

return $(u^*, \mathbf{v}^*) = (u^{t+1}, \mathbf{v}^{t+1})$.

Minimization with respect to u . Fixing an unitary vector field \mathbf{v}^t , the minimization problem (56) is convex with respect to u and the minimization problem can be solved via primal-dual Algorithm 1 without acceleration due to the lack of strong convexity of the projection map \mathcal{S} , which results in a non-smooth dual problem.

Minimization with respect to \mathbf{v} . Fixing u^{t+1} , the minimization problem (57) can be solved by the primal-dual algorithm with

$$F(\mathbf{v}) = \mu \text{TV}(\mathbf{v}) \quad \text{and} \quad G(\mathbf{v}) = \zeta \int_{\Omega} \left(1 - \mathbf{v} \cdot \frac{\nabla u^{t+1}}{|\nabla u^{t+1}|} \right)^2 d\mathbf{x}.$$

Let $\mathbf{s} = K\mathbf{v}$, $K = \nabla$ and $K^* = -\text{div}$. Then, the proximal of F^* , with $F(\mathbf{v}) = \mu \text{TV}(\mathbf{v})$, is the projection onto the polar ball:

$$\mathbf{prox}_{\sigma F^*}(\mathbf{s}) = \frac{\mathbf{s}}{\max(1, \mu^{-1} \|\mathbf{s}\|_2)}.$$

The proximal map of G at $\hat{\mathbf{v}} = (\hat{v}_1, \hat{v}_2)$, for $\mathbf{p} = \nabla u^{t+1} / |\nabla u^{t+1}| = (p_1, p_2)$, reads as

$$\mathbf{prox}_{\tau G}(\hat{\mathbf{v}}) = \arg \min_{\mathbf{v} \in \mathbb{R}^2} \zeta \|1 - \mathbf{v} \cdot \mathbf{p}\|_2^2 + \frac{1}{2\tau} \|\mathbf{v} - \hat{\mathbf{v}}\|_2^2,$$

thus

$$\mathbf{prox}_{\tau G}(\hat{\mathbf{v}}) = \begin{pmatrix} 2\zeta p_1^2 + \tau^{-1} & 2\zeta p_1 p_2 \\ 2\zeta p_1 p_2 & 2\zeta p_2^2 + \tau^{-1} \end{pmatrix}^{-1} \begin{pmatrix} 2\zeta p_1 + \tau^{-1} \hat{v}_1 \\ 2\zeta p_2 + \tau^{-1} \hat{v}_2 \end{pmatrix}.$$

Since G is strongly-convex, we use the accelerated scheme (45), with K instead of \mathcal{K} .

Numerical Results. We tested Algorithm 3 in MATLAB on synthetic and real surfaces. Differently from [31], we did not use CVX or MOSEK, making our approach suitable for larger surfaces, beyond the variable size limit imposed by CVX. In what follows, we will use (49) for solving (56) and we will test both single and joint directional regularisers, namely $\mathbf{a} = (0, 1, 0)$, $\mathbf{a} = (0, 0, 1)$ and $\mathbf{a} = (0, \alpha_{2,0}, \alpha_{3,0})$, with $\alpha_{2,0}$ and $\alpha_{3,0}$ to be chosen appropriately for the situation. For a better visualization of the results, a divergence RGB colormap in the range $([0.230, 0.299, 0.754], [0.706, 0.016, 0.150])$ has been applied.

Pyramid dataset from [31]. A pyramid with height data available on three contour lines and no extra information on the tip is given, so as to test whether our model can reconstruct it. We initialize u^0 and \mathbf{v}^0 randomly. In Figure 10, we report in the first column the location of the available data (top) and the ground truth (bottom); in the second column the random initialization of \mathbf{v}^0 (top) and u^0 (bottom); in the third, fourth and fifth columns we report the results from different orders of directional regularisers, namely $\mathbf{a} = (0, 1, 0)$, $\mathbf{a} = (0, 1, 0)$ and $\mathbf{a} = (0, 1, 1)$, with one level of anisotropy $a = 1$. The similarity of the resulting vector fields in Figure 10, despite the different derivative orders involved in the minimisation with respect to u , shows the robustness of the computation of \mathbf{v} for such problem. Visual results suggest that a combination between second and third order directional regularisers, e.g. $\mathbf{a} = (0, \alpha_{2,0}, \alpha_{3,0})$, is desirable since it smooths the second-order result without losing its features.

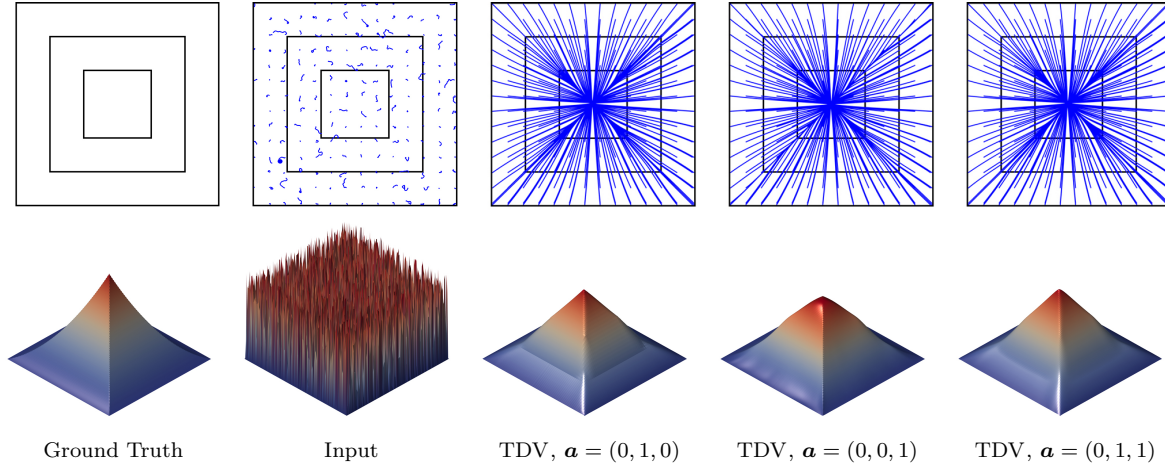


Figure 10: Pyramid results: 10 iterations of [Algorithm 3](#). Parameters: $\eta = 100$, $\mu = \zeta = 1$.

SRTM dataset from [48]. This dataset is part of the *Shuttle Radar Topography Mission* (SRTM) [48] NASA mission conducted in 2000 to obtain elevation data for most areas of the world. We download `.hgt` “height” binary data files from [6], where by selection of latitude and longitude coordinates we get 1×1 degree tiles of 1-arc seconds resolution (around 30 m per pixel). We selected some famous mountains within Italy: Etna volcano (Sicily), Baldo Mountain (Verona), Vesuvio volcano (Naples), Brenner border (Sterzing) and Gran Sasso (L’Aquila), labelled from S1 to S5 in [Figure 11](#), whose image size domain is 250×250 pixels. As input, we randomly selected approximately 7% of sparse data on level lines and isolated points with parameters $Q = 3$, anisotropy $a = 1$ and $\mathbf{a} = (0, 0.1, 1)$.

Atomic Force Microscopy dataset from [40]. Atomic force microscopy (AFM), or scanning probe microscopy (SPM), is a topography imaging technique which scans objects at high resolution while recording the topographical information, commonly used in the detection of cancer cells in cellular biology. In [37], the study of a compressed sensing approach on AFM images was motivated by the reduction of the image acquisition time for multiple reasons, e.g. to minimize the operator time spent at the equipment [26], to allow time-dependent dynamic processes [43] and to minimize the interaction of instruments with specimens so as to reduce potential risks of damages [35]. Therefore, the authors proposed to speed up the sampling procedure by scanning height data on spirals rather than exploring pixel by pixel, so as to reconstruct the missing data via compressed sensing. The authors define the under-sampling ratio as $\rho = L/L_{ref}$, where L is the length of the spiral path followed by the probe for acquiring the data and L_{ref} is the distance travelled by the probe in pixels during the raster scan. Note that L also counts the path outside the imaging domain due to smooth movement requirement of the probe, while L_{ref} is approximated by the value $2 \cdot \#\text{pixels}$ and the factor of two is due by the the usual approach to acquire two topography buffers, even if only one is used for the visualization. In order to test our reconstruction method based on the directional regularisers, we downloaded the open source AFM `.mi` dataset of 512×512 height values from [40], exported

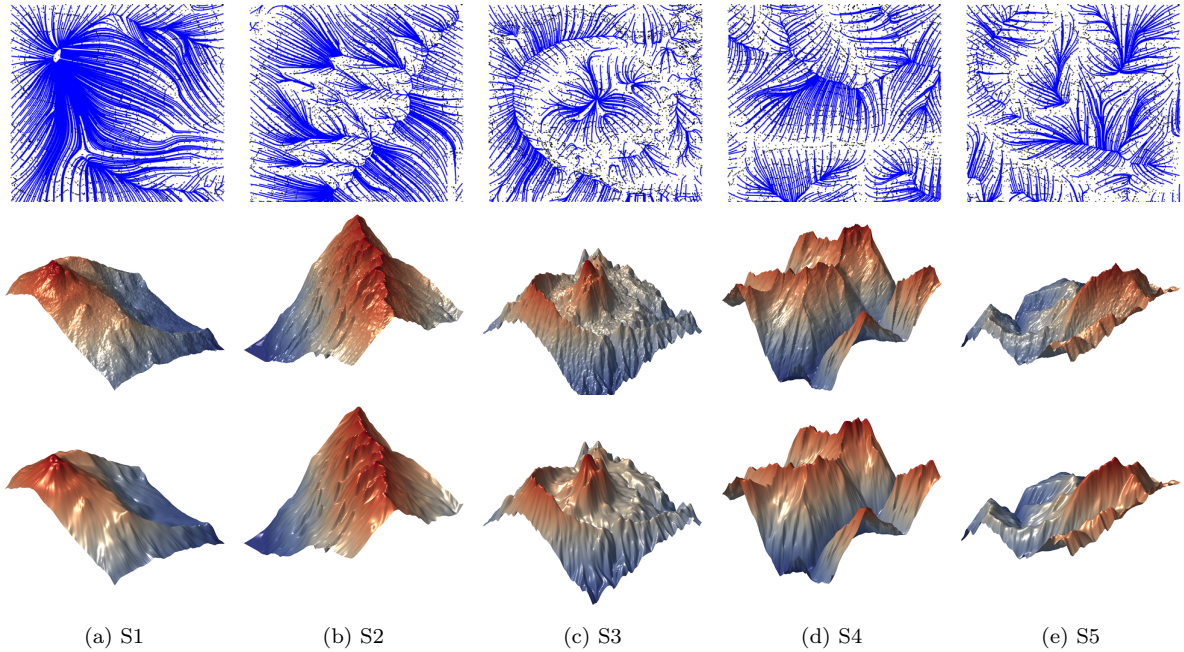


Figure 11: The dataset from [48]. First row: height location (black), streamlines of v (blue). Second row: ground truth. Third Row: TDV results, $\mathbf{a} = (0, 0.1, 1)$, $\mu = \zeta = 1$, $\eta = 1000$.

in ASCII text via the open-source software Gwyddion and imported in MATLAB. Our input are AFM surfaces of size 256×256 obtained by slicing the original surface, for comparison purposes following [37]. We show the results in Figure 12 for the ground truth image in Figure 12a, with different under-sampling ratio ρ , see Figures 12c and 12d. In Figure 12b we compare the structural similarity indicator (SSIM) [49] for our results with [37, Figure 7], where iterative hard thresholding (IHT), iterative soft thresholding (IST) and their weighted version (w-IHT and w-IST) were tested: we conclude that our approach is robust throughout different under-sampled data, with good quality surfaces in terms of SSIM.

6. Conclusions. In this work, we have shown that embedding anisotropic directional information into higher order derivatives improves the performance of total variation regularization in many imaging applications where anisotropy plays a crucial role. In particular, we present results for image denoising, image zooming and interpolation of scattered measurements, with details on the numerical discretisation and the solution via a primal-dual hybrid gradient algorithm. With this we provided a precise discrete framework which extends the works [31, 20, 11, 10], bringing higher-order total variation together with spatially-varying anisotropy. The continuous model will be analysed in the second part of this work [39],

Acknowledgements. The authors are grateful to Dr. Martin Holler, University of Graz (Austria) for the useful discussions and to Prof. Thomas Arildsen, Aalborg University (Denmark) for the AFM data.

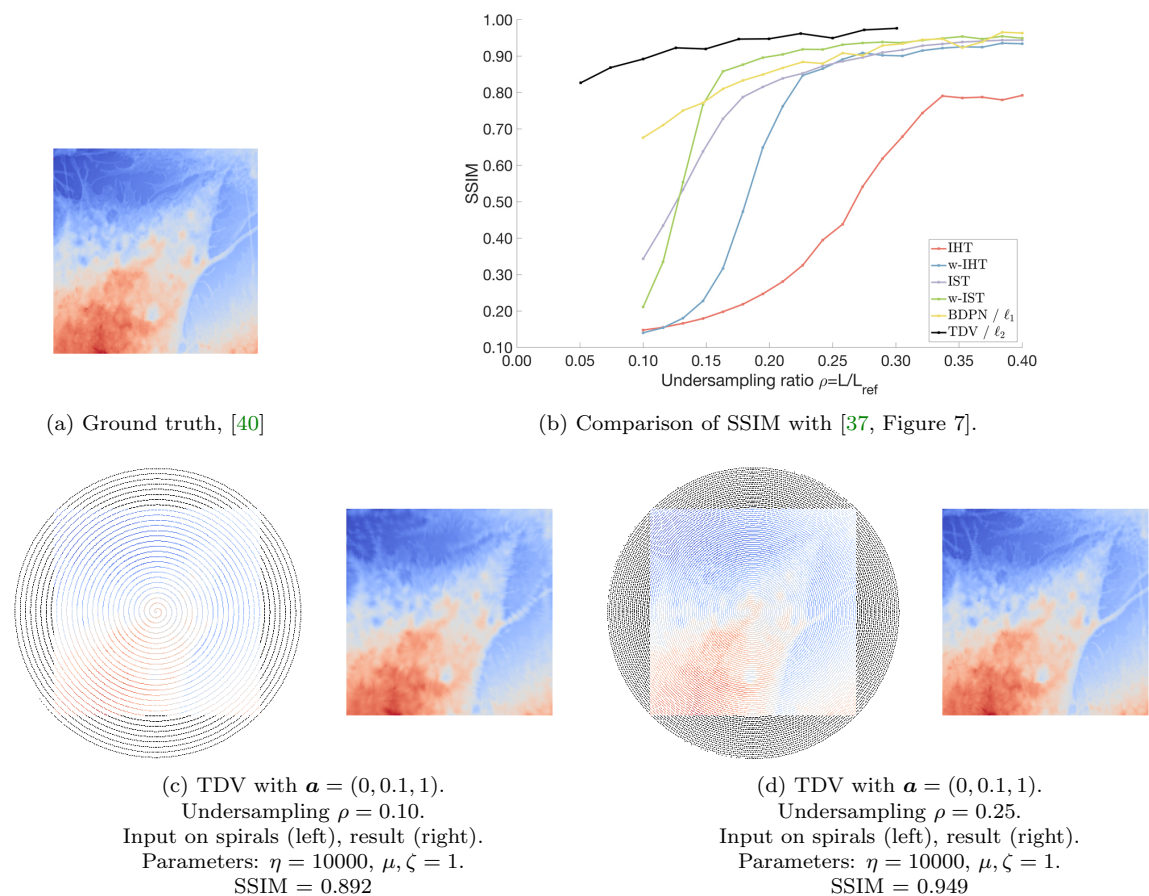


Figure 12: AFM reconstruction with Algorithm 3.

REFERENCES

- [1] T. AACH, C. MOTA, I. STUKE, M. MUHLICH, AND E. BARTH, *Analysis of superimposed oriented patterns*, IEEE Transactions on Image Processing, 15 (2006), pp. 3690–3700, <https://doi.org/10.1109/TIP.2006.884921>.
- [2] A. ALMANSA, F. CAO, Y. GOUSSEAU, AND B. ROUGE, *Interpolation of digital elevation models using amle and related methods*, IEEE Transactions on Geoscience and Remote Sensing, 40 (2002), pp. 314–325, <https://doi.org/10.1109/36.992791>.
- [3] L. ALVAREZ, F. GUICHARD, P.-L. LIONS, AND J.-M. MOREL, *Axioms and fundamental equations of image processing*, Archive for Rational Mechanics and Analysis, (1993).
- [4] C. BALLESTER, M. BERTALMIO, V. CASELLES, G. SAPIRO, AND J. VERDERA, *Filling-in by joint interpolation of vector fields and gray levels*, IEEE Transactions on Image Processing, 10 (2001), pp. 1200–1211, <https://doi.org/10.1109/83.935036>.
- [5] I. BAYRAM AND M. E. KAMASAK, *Directional total variation*, IEEE Signal Processing Letters, 19 (2012), pp. 781–784, <https://doi.org/10.1109/LSP.2012.2220349>.
- [6] F. BEAUDUCEL, *Readhgt: Import/download nasa srtm data files (.hgt)*, 2012, <https://www.mathworks.com/matlabcentral/fileexchange/36379>.

- [7] B. BERKELS, M. BURGER, M. DROSKE, O. NEMITZ, AND M. RUMPF, *Cartoon Extraction Based on Anisotropic Image Classification*, in Vision, Modeling, and Visualization Proceedings, 2006, pp. 293–300, <http://numod.ins.uni-bonn.de/research/papers/public/BeBuDr06.pdf>.
- [8] T. R. BIN WU AND X.-C. TAI, *Sparse-data based 3d surface reconstruction for cartoon and map*, Internal report, UCLA, (2017), <ftp://ftp.math.ucla.edu/pub/camreport/cam17-38.pdf>.
- [9] P. BLOMGREN AND T. F. CHAN, *Color tv: total variation methods for restoration of vector-valued images*, IEEE Transactions on Image Processing, 7 (1998), pp. 304–309, <https://doi.org/10.1109/83.661180>.
- [10] K. BREDIES AND M. HOLLER, *A TGV Regularized Wavelet Based Zooming Model*, Springer, 2013, pp. 149–160, https://doi.org/10.1007/978-3-642-38267-3_13.
- [11] K. BREDIES, K. KUNISCH, AND T. POCK, *Total generalized variation*, SIAM Journal on Imaging Sciences, 3 (2010), pp. 492–526, <https://doi.org/10.1137/090769521>.
- [12] V. CASELLES, A. CHAMBOLLE, D. CREMERS, M. NOVAGA, AND T. POCK, *An introduction to total variation for image analysis*, Theoretical Foundations and Numerical Methods for Sparse Recovery, 9 (2010), pp. 263–340, <https://doi.org/10.1515/9783110226157.263>.
- [13] V. CASELLES, A. CHAMBOLLE, AND M. NOVAGA, *The discontinuity set of solutions of the tv denoising problem and some extensions*, Multiscale Modeling & Simulation, 6 (2007), pp. 879–894, <https://doi.org/10.1137/070683003>.
- [14] V. CASELLES, B. TANG, AND G. SAPIRO, *Direction diffusion*, in Proceedings of the Seventh IEEE International Conference on Computer Vision (ICCV), vol. 02, 09 1999, p. 1245, <https://doi.org/10.1109/ICCV.1999.790423>.
- [15] A. CHAMBOLLE AND T. POCK, *A first-order primal-dual algorithm for convex problems with applications to imaging*, Journal of Mathematical Imaging and Vision, 40 (2011), pp. 120–145, <https://doi.org/10.1007/s10851-010-0251-1>.
- [16] A. CHAMBOLLE AND T. POCK, *An introduction to continuous optimization for imaging*, Acta Numerica, 25 (2016), pp. 161–319, <https://doi.org/10.1017/S096249291600009X>.
- [17] T. CHAN, S. ESEDOGLU, AND F. PARK, *A fourth order dual method for staircase reduction in texture extraction and image restoration problems*, in 2010 IEEE International Conference on Image Processing, 2010, pp. 4137–4140, <https://doi.org/10.1109/ICIP.2010.5653199>.
- [18] T. CHAN, A. MARQUINA, AND P. MULET, *High-order total variation-based image restoration*, SIAM Journal on Scientific Computing, 22 (2000), pp. 503–516, <https://doi.org/10.1137/S1064827598344169>.
- [19] K. DABOV, A. FOI, V. KATKOVNIK, AND K. EGIAZARIAN, *Image denoising by sparse 3-d transform-domain collaborative filtering*, IEEE Transactions on Image Processing, 16 (2007), pp. 2080–2095, <https://doi.org/10.1109/TIP.2007.901238>.
- [20] R. DALGAS KONGSKOV, Y. DONG, AND K. KNUDSEN, *Directional Total Generalized Variation Regularization*, ArXiv e-prints, (2017), <https://arxiv.org/abs/1701.02675>.
- [21] Y. DONG AND M. HINTERMÜLLER, *Multi-scale Total Variation with Automated Regularization Parameter Selection for Color Image Restoration*, Springer, 2009, pp. 271–281, https://doi.org/10.1007/978-3-642-02256-2_23.
- [22] M. J. EHRHARDT AND M. M. BETCKE, *Multicontrast mri reconstruction with structure-guided total variation*, SIAM Journal on Imaging Sciences, 9 (2016), pp. 1084–1106, <https://doi.org/10.1137/15M1047325>.
- [23] V. ESTELLERS, S. SOATTO, AND X. BRESSON, *Adaptive regularization with the structure tensor*, IEEE Transactions on Image Processing, 24 (2015), pp. 1777–1790, <https://doi.org/10.1109/TIP.2015.2409562>.
- [24] W. FÖRSTNER, *A feature based correspondence algorithm for image matching*, Int. Arch. of Photogrammetry and Remote Sensing, 26 (1986), pp. 150–166.
- [25] M. GRASMAIR AND F. LENZEN, *Anisotropic total variation filtering*, Applied Mathematics and Optimization, 62 (2010), pp. 323–339, <https://doi.org/10.1007/s00245-010-9105-x>.
- [26] P. K. HANSMA, G. SCHITTER, G. E. FANTNER, AND C. PRATER, *High-speed atomic force microscopy*, Science, 314 (2006), pp. 601–602, <https://doi.org/10.1126/science.1133497>.
- [27] C. HARRIS AND M. STEPHENS, *A combined corner and edge detector*, in Proceedings of the Alvey Vision Conference, Alvey Vision Club, 1988, pp. 23.1–23.6, <https://doi.org/10.5244/C.2.23>.
- [28] M. KASS AND A. WITKIN, *Analyzing oriented patterns*, Computer Vision, Graphics, and Image Processing, 37 (1987), pp. 362–385, [https://doi.org/10.1016/0734-189X\(87\)90043-0](https://doi.org/10.1016/0734-189X(87)90043-0).

- [29] R. KIMMEL, R. MALLADI, AND N. SOCHEN, *Images as embedded maps and minimal surfaces: Movies, color, texture, and volumetric medical images*, International Journal of Computer Vision, 39 (2000), pp. 111–129, <https://doi.org/10.1023/A:1008171026419>.
- [30] S. LEFKIMMIATIS, A. ROUSSOS, P. MARAGOS, AND M. UNSER, *Structure tensor total variation*, SIAM Journal on Imaging Sciences, 8 (2015), pp. 1090–1122, <https://doi.org/10.1137/14098154X>.
- [31] J. LELLMANN, J.-M. MOREL, AND C.-B. SCHÖNLIEB, *Anisotropic third-order regularization for sparse digital elevation models*, in Scale Space and Variational Methods in Computer Vision, Springer, 2013, pp. 161–173, https://doi.org/10.1007/978-3-642-38267-3_14.
- [32] F. LENZEN, F. BECKER, J. LELLMANN, S. PETRA, AND C. SCHNÖRR, *A class of quasi-variational inequalities for adaptive image denoising and decomposition*, Computational Optimization and Applications, 54 (2013), pp. 371–398, <https://doi.org/10.1007/s10589-012-9456-0>.
- [33] R. LEONID, S. OSHER, AND E. FATEMI, *Nonlinear total variation based noise removal algorithms*, Physica D: Nonlinear Phenomena, 60 (1992), pp. 259 – 268, [https://doi.org/10.1016/0167-2789\(92\)90242-F](https://doi.org/10.1016/0167-2789(92)90242-F).
- [34] J. MEINGUET, *Surface Spline Interpolation: Basic Theory and Computational Aspects*, Springer, 1984, pp. 127–142, https://doi.org/10.1007/978-94-009-6466-2_6.
- [35] D. MÜLLER AND Y. DUFRÈNE, *Atomic force microscopy: a nanoscopic window on the cell surface*, Trends in Cell Biology, 21 (2011), pp. 461 – 469, <https://doi.org/10.1016/j.tcb.2011.04.008>.
- [36] M. NIKOLOVA, *Local strong homogeneity of a regularized estimator*, SIAM Journal on Applied Mathematics, 61 (2000), pp. 633–658, <https://doi.org/10.1137/S0036139997327794>.
- [37] C. S. OXVIG, T. ARILDSEN, AND T. LARSEN, *Structure assisted compressed sensing reconstruction of undersampled afm images*, Ultramicroscopy, 172 (2017), pp. 1–9, <https://doi.org/10.1016/j.ultramic.2016.09.011>.
- [38] K. PAPAITSOROS AND C. SCHÖNLIEB, *A combined first and second order variational approach for image reconstruction*, Journal of Mathematical Imaging and Vision, 48 (2014), pp. 308–338, <https://doi.org/10.1007/s10851-013-0445-4>.
- [39] S. PARISOTTO, S. MASNOU, AND C. B. SCHÖNLIEB, *Higher order total directional variation. Part II: Analysis*, arXiv e-prints, (2018).
- [40] C. RANKL, *Atomic force microscopy images of cell specimens*, 2015, <https://doi.org/10.5281/zenodo.17573>.
- [41] G. SAPIRO AND D. L. RINGACH, *Anisotropic diffusion of multivalued images with applications to color filtering*, IEEE Transactions on Image Processing, 5 (1996), pp. 1582–1586, <https://doi.org/10.1109/83.541429>.
- [42] O. SAVIN, *C^1 regularity for infinity harmonic functions in two dimensions*, Archive for Rational Mechanics and Analysis, 176 (2005), pp. 351–361, <https://doi.org/10.1007/s00205-005-0355-8>.
- [43] G. SCHITTER AND M. ROST, *Scanning probe microscopy at video-rate*, Materials Today, 11 (2008), pp. 40–48, [https://doi.org/10.1016/S1369-7021\(09\)70006-9](https://doi.org/10.1016/S1369-7021(09)70006-9).
- [44] S. SETZER AND G. STEIDL, *Variational methods with higher-order derivatives in image processing*, Approximation XII, (2008), pp. 360–386.
- [45] S. SETZER, G. STEIDL, AND T. TEUBER, *Infimal convolution regularizations with discrete l_1 -type functionals*, Communications in Mathematical Sciences, 9 (2011), pp. 797–827, <https://doi.org/10.1.1.572.6214>.
- [46] G. STEIDL AND T. TEUBER, *Anisotropic Smoothing Using Double Orientations*, Springer, 2009, pp. 477–489, https://doi.org/10.1007/978-3-642-02256-2_40.
- [47] D. TSCHUMPERLE AND R. DERICHE, *Vector-valued image regularization with pdes: a common framework for different applications*, IEEE Transactions on Pattern Analysis and Machine Intelligence, 27 (2005), pp. 506–517, <https://doi.org/10.1109/TPAMI.2005.87>.
- [48] USGS, *Shuttle Radar Topography Mission*, 2006, <https://www2.jpl.nasa.gov/srtm/>.
- [49] Z. WANG, A. C. BOVIK, H. R. SHEIKH, AND E. P. SIMONCELLI, *Image quality assessment: from error visibility to structural similarity*, IEEE Transactions on Image Processing, 13 (2004), pp. 600–612, <https://doi.org/10.1109/TIP.2003.819861>.
- [50] J. WEICKERT, *Anisotropic diffusion in image processing*, 1998.
- [51] J. WEICKERT, *Coherence-enhancing diffusion filtering*, International Journal of Computer Vision, 31 (1999), pp. 111–127, <https://doi.org/10.1023/A:1008009714131>.
- [52] C. WU AND X.-C. TAI, *Augmented lagrangian method, dual methods, and split bregman iteration for*

- rof, vectorial tv, and high order models*, SIAM Journal on Imaging Sciences, 3 (2010), pp. 300–339, <https://doi.org/10.1137/090767558>.
- [53] S. D. ZENZO, *A note on the gradient of a multi-image*, Computer Vision, Graphics, and Image Processing, 33 (1986), pp. 116 – 125, [https://doi.org/10.1016/0734-189X\(86\)90223-9](https://doi.org/10.1016/0734-189X(86)90223-9).
- [54] H. ZHANG AND Y. WANG, *Edge adaptive directional total variation*, The Journal of Engineering, (2013), <https://doi.org/10.1049/joe.2013.0116>.